Received: 17 January 2019 | Revised: 23 May 2019 | Accepted: 27 June 2019
DOI: 10.1002/joc.6219

RESEARCH ARTICLE

International Journal of Climatology RMetS

The Central Chile Mega Drought (2010–2018): A climate dynamics perspective

René D. Garreaud[1,2] | Juan P. Boisier[2] | Roberto Rondanelli[1,2] | Aldo Montecinos[3,4] | Hector H. Sepúlveda[3] | Daniel Veloso-Aguila[3]

[1]Geophysics Department, Universidad de Chile, Santiago, Chile
[2]Center for Climate and Resilience Research, Universidad de Chile, Santiago, Chile
[3]Department of Geophysics, Universidad de Concepción, Concepción, Chile
[4]Centro de Recursos Hídricos para la Agricultura y Minería, Universidad de Concepción, Concepción, Chile

Correspondence
René D. Garreaud, Blanco Encalada 2002, Santiago, Chile.
Email: rgarreau@dgf.uchile.cl

Funding information
CONICYT Chile, Grant/Award Numbers: FONDAP 15110009, FONDECYT 1170286

Abstract
Central Chile, home to more than 10 million inhabitants, has experienced an uninterrupted sequence of dry years since 2010 with mean rainfall deficits of 20–40%. The so-called Mega Drought (MD) is the longest event on record and with few analogues in the last millennia. It encompasses a broad area, with detrimental effects on water availability, vegetation and forest fires that have scaled into social and economical impacts. Observations and reanalysis data reveal that the exceptional length of the MD results from the prevalence of a circulation dipole-hindering the passage of extratropical storms over central Chile—characterized by deep tropospheric anticyclonic anomalies over the subtropical Pacific and cyclonic anomalies over the Amundsen–Bellingshausen Sea. El Niño Southern Oscillation (ENSO) is a major modulator of such dipole, but the MD has occurred mostly under ENSO-neutral conditions, except for the winters of 2010 (La Niña) and 2015 (strong El Niño). Climate model simulations driven both with historical forcing (natural and anthropogenic) and observed global SST replicate the south Pacific dipole and capture part of the rainfall anomalies. Idealized numerical experiments suggest that most of the atmospheric anomalies emanate from the subtropical southwest Pacific, a region that has experienced a marked surface warming over the last decade. Such warming may excite atmospheric Rossby waves whose propagation intensifies the circulation pattern leading to dry conditions in central Chile. On the other hand, anthropogenic forcing (greenhouse gases concentration increase and stratospheric ozone depletion) and the associated positive trend of the Southern Annular Mode also contribute to the strength of the south Pacific dipole and hence to the intensity and longevity of the MD. Given the concomitance of the seemingly natural (ocean sourced) and anthropogenic forcing, we anticipate only a partial recovery of central Chile precipitation in the decades to come.

KEYWORDS
Chile, climate change, drought, ENSO, PDO, SAM, South America

1 | INTRODUCTION

When will a drought break? This is a pressing question posed by stakeholders—from local farmers to national water authorities—during prolonged dry periods. Progress towards its answer requires disentangling the role of natural climate variability and anthropogenic climate change in sustaining precipitation scarcity at a regional scale. On interannual time-scales, El Niño Southern Oscillation (ENSO) is the leading driver of droughts in many regions worldwide (e.g., Vicente-Serrano *et al*., 2011; Schubert *et al*., 2016) followed by other ocean-forced modes of variability or by land surface processes (Seneviratne *et al*., 2012). On the other hand, there is mounting evidence that climate change is already increasing the frequency, duration and intensity of regional droughts (e.g., Dai, 2011; 2013), by either inducing circulation-mediated precipitation deficit or enhancing evapotranspiration. If one concludes that a given drought is mostly of natural origin, reversal towards normal or even wetter conditions should occur in the foreseeable future even though one cannot predict the exact time of such shift. If, by the contrary, global warming is the main driver of the rainfall deficit, one should expect (and adapt to) a sustained trend towards drier conditions.

Intense, short-lived (1–2 years) droughts are a rather common feature in Mediterranean-like climates (where most of the annual rainfall is accounted for in a few winter storms) but during the last decades, these regions have also experienced much longer dry spells. The multi-year (2012–2014) drought in California attracted considerable interest (e.g., Griffin and Anchukaitis, 2014; Swain, 2015; Williams *et al*., 2015) given its unprecedented effects in hydrology, forest fires and agriculture (e.g., AghaKouchak *et al*., 2014; Mao *et al*., 2015). The lack of winter rainfall over that region was directly associated with an anomalously persistent high-pressure ridge over the northeast Pacific that in turn appears as a response to tropical sea-surface temperature (SST) anomalies of mostly natural origin (Seager *et al*., 2015). A decade-long drought also afflicted southeastern Australia in the recent past (ca. 1997–2009, Saft *et al*., 2015) disrupting river ecosystems and agricultural production as reviewed in van Dijk *et al*. (2013). The rainfall deficit during the so-called Millennium Drought has been partially attributed to climate change -specifically to anthropogenic greenhouse warming—throughout a trend in the Southern Annular Mode (SAM) towards its positive polarity and a poleward shift of the Hadley Cell (Cai *et al*., 2014). Multi-year rainfall deficits have also prevailed recently in-land areas surrounding the Mediterranean Sea (Garcia-Herrera *et al*., 2007; Hoerling *et al*., 2010), South Africa (Rouault and Richard, 2003) and the Middle East (Trigo *et al*., 2010; Kelley *et al*., 2015).

Central Chile, along the west coast of South America (30°–38°S, Figure 1), exhibits an archetypical Mediterranean climate (e.g., Miller, 1976) with annual mean precipitation ranging between 100 and 2000 mm (Viale and Garreaud, 2015), mostly concentrated in austral winter (May–September) and produced by cold fronts (Falvey and Garreaud, 2007; Viale and Nuñez, 2011). The interannual rainfall variability is large (coefficient of variation about 0.3) and partially driven by ENSO (e.g., Aceituno, 1988; Montecinos and Aceituno, 2003; see also Section 4.2). A regional drying trend, of particularly large magnitude since the late 1970s, but observed since the mid-20th century (Quintana and Aceituno, 2012; Masiokas *et al*., 2016; Boisier *et al*., 2018), has been partially attributed to anthropogenic climate change (Vera and Díaz, 2015; Boisier *et al*., 2016; 2018). Such trend is expected to continue in the future, as model-based regional climate projections consistently indicate a reduction in mean annual precipitation (up to 40% relative to current values) for the second half of this century under high emission scenarios (Fuenzalida *et al*., 2007; Bozkurt *et al*., 2018).

The observed decline of precipitation over central Chile has been greatly accentuated by an uninterrupted sequence of dry years since 2010 to the present, with annual rainfall deficits ranging between 25 and 45%. This ongoing, multi-year dry spell has been referred to as the Central Chile Mega Drought (MD; CR2, 2015) owing to its unprecedented longevity and large spatial extent in the historical record. The MD impacts on hydroclimate and vegetation are described in Garreaud *et al*. (2017). The precipitation deficit resulted in the diminished Andean snowpack, reservoir volumes and groundwater levels across central Chile. Mean river discharge decreased up to 90% as well as nutrient exportation into the sea with potential impacts on coastal ecology (Masotti *et al*., 2018). The hydrological drought also extended into westernmost Argentina (Rivera *et al*., 2017). A substantial decrease in vegetation productivity was observed in the shrubland-dominated, northern sector of central Chile, but a mix of greening and browning patches occurred farther south where irrigated croplands and exotic forest plantations dominate. The MD coincided with the warmest decade on record, leading to a substantial increase (~60%) of the burned area by forest fires (González *et al*., 2018). The biophysical impacts of the MD ultimately resulted in detrimental consequences for the Chilean population (~70% of which reside in Central Chile), especially in rural areas (Aldunce *et al*., 2017). Such social distress was recognized by county, regional and national authorities, that took several but weakly coordinated measures during the MD (Verbist *et al*., 2016).

The seemingly unprecedented character of the ongoing MD and the prospect of a drier climate emphasize our initial query. To this end, we investigate the large-scale circulation patterns and physical mechanisms sustaining the protracted dry conditions in central Chile during 2010–2018. Observations and model simulations are described in Section 2. We

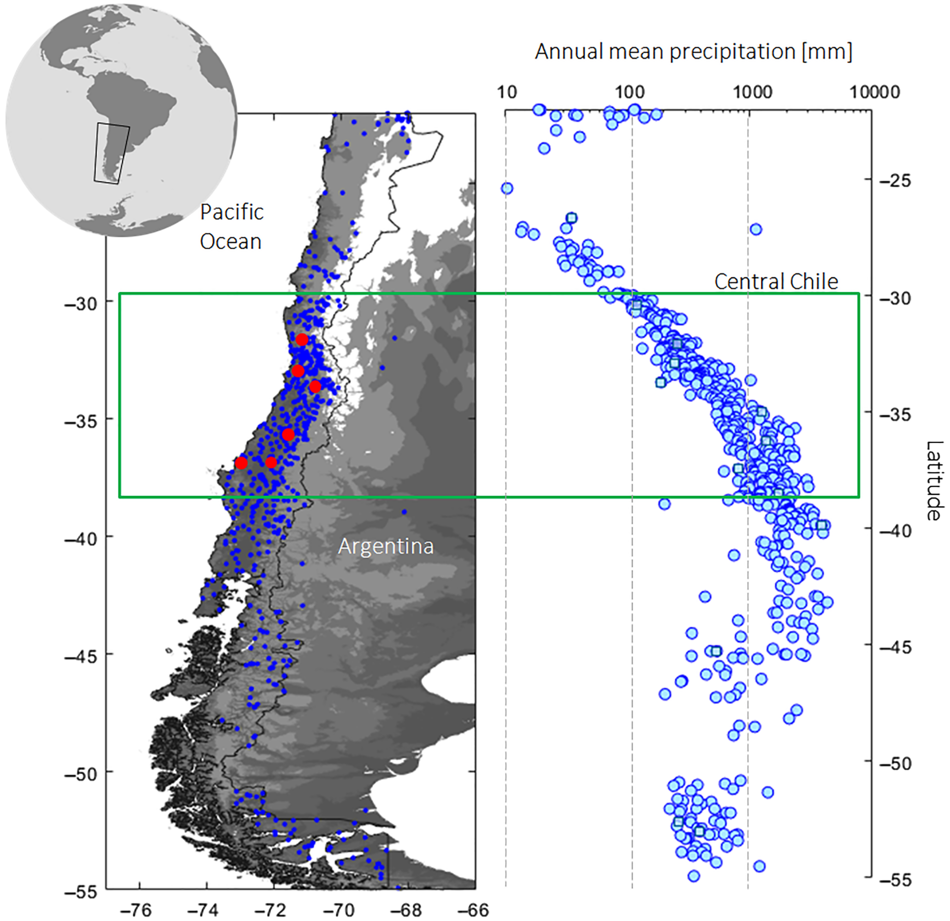

FIGURE 1 Geographic and climate features of Central Chile. (a) Topographic map (dark grey: Terrain elevation <500 m asl; light grey: 500–3,000 m asl; white: > 3,000 m asl). Blue dots are rain gauges stations operated by DMC/DGA. Red circles are the location of the six stations used to define the regional precipitation index. Stations that provide records for Figure 4 are also indicated. (b) Station-based annual mean rainfall (1980–2010) according to latitude [Colour figure can be viewed at wileyonlinelibrary.com]

then provide a brief description of the observed precipitation anomalies in central Chile (Section 3), updating a more comprehensive analysis in Garreaud *et al*. (2017). Atmospheric reanalysis are used in Section 4 to describe the large-scale circulation anomalies during the current MD and past droughts during the 20th century. We also evaluated the historical and present-day association between central Chile rainfall and relevant planetary-scale modes (ENSO, SAM and the Pacific Decadal Oscillation, PDO) to infer their role during the MD. To assess natural and anthropogenic contributions to the current MD, in Section 5, we use a large ensemble of Global Climate Model (GCM) data, including both fully-coupled runs and simulations with prescribed SST. Additional numerical experiments were conducted to isolate the ocean-sourced forcing of the dry conditions in central Chile and propose a physical mechanism for such connection. Conclusions are summarized in Section 6.

2 | DATA AND MODELS

2.1 | Observational dataset

Several sources of information are used to characterize central Chile historical droughts and the current event. At the regional scale, the Chilean Directorate of water resources (DGA) and the National Weather Service (DMC) maintain more than 500 rain gauges along central Chile (Figure 1). From the original daily observations, we computed monthly accumulations when less than 5% of the days are missing, thus retaining 220 stations with data from 1960 onwards. We also use lake and groundwater levels in a few stations operated by DGA. All the station data is available from the Center for Climate and Resilience Research Climate Explorer (http://explorador.cr2.cl).

The large-scale circulation was characterized using the National Centers for Environmental Prediction—National Center for Atmospheric Research (NCEP-NCAR) reanalysis (NNR; Kalnay *et al*., 1996) available since 1948, including gridded (2.5° × 2.5° latitude–longitude [lat–lon]) monthly means of geopotential height and air temperature at several levels. NNR-based results were contrasted against the European Centre for Medium-Range Weather Forecasts ERA-Interim Reanalysis (Dee *et al*., 2011). Our study also employs monthly mean SST fields from the NOAA extended-reconstructed sea surface temperature (ERSST) available from 1860 onwards on a 2° × 2° lat–lon grid (Smith *et al*., 2008) and the NOAA Optimum Interpolation (OI) SST - V2 available from 1981 onwards on a 1° × 1°

lat–lon grid (Reynolds *et al*., 2002). Global precipitation is depicted using monthly mean fields from the Global Precipitation Climatology Project (GPCP) available from 1979 to present on a 2.5° × 2.5° lat–lon grid (Adler *et al*., 2003).

2.2 | Atmospheric only simulations

In Section 5, we use several families of GCM simulations to gauge the role of natural variability and anthropogenic forcing in sustaining the ongoing MD. First, we use a 40-member ensemble carried out with the Community Atmosphere Model (CAM5, the atmospheric component of the Community Earth System Model, Kay *et al*., 2015) by the NOAA Earth System Research Laboratory. CAM5 was integrated from January 1900 to February 2018 at approximately 1° × 1° lat–lon resolution, forced by observed SST and Sea Ice (Hurrell *et al*., 2008). These kind of simulations, with prescribed ocean boundary conditions, are referred to as AMIP as they were employed in the Atmospheric Model Intercomparison Project (Gates *et al*., 1998). They also employ time-varying greenhouse gases (GHG) and stratospheric ozone (O_3) concentrations. The GHG evolution is based on observed estimates until 2005 and the RCP6.0 scenario thereafter (Moss *et al*., 2010). The time-varying O_3 is from the SPARC observed database (Cionni *et al*., 2011). Consistently, this simulation is referred to as AMIP-ORF (observed radiative forcing). Note that these simulations include 8 out of 9 winters of the ongoing MD. Since the ensemble members are forced by identical boundary conditions and only differ in slightly different initial conditions, the *ensemble mean* attempts to isolate the SST-forced response of the atmospheric circulation under observed levels of GHG and O3 while the *ensemble spread* informs about the SST-forced signal to internal atmospheric noise ratio.

A second set of AMIP simulations, also performed with CAM5, consists of a 30-member ensemble spanning January 1979 to December 2016, but with GHG and O_3 concentrations kept fixed to their 1880s values (Cionni *et al*., 2011; Meinshausen *et al*., 2011). In this case, SST has been detrended and adjusted to 1880 equivalent mean conditions, but retain the observed interannual and decadal variability as in the other experiments. Sea ice is set to a repeating seasonal cycle of roughly 1979–1990. This set of simulations is referred to as AMIP-PRF (past radiative forcing) and attempts to reproduce the atmospheric circulation in response to natural SST variability previous to major human interference in the climate system. Thus, comparing AMIP-PRF against AMIP-ORF is useful to precisely gauge that interference.

2.3 | Fully-coupled GCM simulations

We used a total of 30 fully-coupled simulations from 26 GCMs participating in CMIP5 (Taylor *et al*., 2012), including three runs from the Community Earth System Model CESM1, that used time-varying GHG and O_3 concentrations (Cionni *et al*., 2011). Table 1 presents the basic features of these simulations. For each CMIP5 model, we combine their historical runs (1950–2005) and RCP8.5 scenario runs (2006–2040). Since averaging across the models/runs effectively removes internal variability, the *multi-model mean* isolates the signal due to anthropogenic climate forcing. We refer to these simulations as CMIP5.

2.4 | SPEEDY experiments

SPEEDY (*Simplified Parameterizations*, *primitivE-Equation DYnamics*) is an atmospheric global circulation model (AGCM) of intermediate complexity. It is based on the primitive equations with a spectral dynamical core and simplified physical parameterizations (Kucharski *et al*., 2013). It is a hydrostatic model with a spectral transformation in the vorticity-divergence form described by Bourke (1974). The model resolution used is T30 L8, which corresponds to a triangular spectral truncation with 30 wave numbers (96 × 48 Gaussian grid points), about 3.75° × 3.75°, and eight vertical levels. The top two upper levels represent the stratosphere, the lowest level the planetary boundary layer and three levels of free troposphere (Molteni, 2003; Kucharski *et al*., 2006). Physical parameterizations include large-scale condensation, short- and longwave radiation, shallow and deep convection, surface fluxes of momentum and energy, and vertical diffusion.

In addition to topography and land–sea mask, SPEEDY requires surface boundary conditions at the ocean (SST and sea ice fraction coverage [SIC]), soil temperature in the deep soil layer (1 m), moisture in the top soil layer and the root-zone layer, snow depth, bare surface albedo, and fraction of land-surface covered by vegetation. The last two levels are defined with an annual mean value, while the other fields are defined as monthly means, which are linearly interpolated to get daily values during the calculation. The climatological fields were originally calculated averaging the 1979–2008 period from ERA-Interim results (Dee *et al*., 2011). For the SPEEDY AMIP run, we prescribed global monthly observed SST and SIC from 1870 to 2017 (Rayner *et al*., 2003). A total of 50 ensemble members for each run were created by adding random diabatic forcing. Ensemble member 1 was perturbed 1 day (72 time steps), ensemble member 2 was perturbed for 2 days, and so on. We also employed SPEEDY to conduct a numerical experiment described at the end of Section 5.1.

3 | REGIONAL FEATURES OF THE MEGA DROUGHT

Despite of marked meridional rainfall gradients, year-to-year precipitation and streamflow variability exhibit a notable

TABLE 1 Main features of the fully coupled models used for the historical and RCP8.5 scenario (Taylor *et al*., 2012)

Model	N_{lon}	N_{lat}	Institution
ACCESS1-0	192	144	CSIRO (Commonwealth Scientific and Industrial Research Organization, Australia), and BOM (Bureau of Meteorology, Australia)
ACCESS1-3	192	144	
Bcc-csm1-1	128	64	Beijing Climate Center(BCC),China Meteorological Administration, China
CanESM2	128	64	CCCma (Canadian Centre for Climate Modelling and Analysis, Victoria, BC, Canada)
CCSM4	288	192	NCAR (National Center for Atmospheric Research) Boulder, CO, USA
CESM1-BGC	288	192	NSF/DOE NCAR (National Center for Atmospheric Research) Boulder, CO, USA
CESM1-CAM5	288	192	
CMCC-CESM	96	48	CMCC—Centro Euro-Mediterraneo per i Cambiamenti Climatici, Bologna, Italy
CNRM-CM5	256	128	CNRM (Centre National de Recherches Meteorologiques, Meteo-France, Toulouse, France)
CSIRO-Mk3-6-0	192	96	CSIRO (Commonwealth Scientific and Industrial Research Organization, Australia), and University of Queensland, Australia
FGOALS-s2	128	108	IAP (Institute of Atmospheric Physics), CAS (Chinese Academy of Sciences), Beijing, China
FIO-ESM	128	64	FIO (The First Institution of Oceanography, SOA, Qingdao, China)
GFDL-CM3	144	90	NOAA GFDL (Geophysical Fluid Dynamics Laboratory, USA)
GFDL-ESM2G	144	90	
GISS-E2-H	144	89	NASA/GISS (Goddard Institute for Space Studies) New York, NY
HadGEM2-CC	192	144	Met Office Hadley Centre, Fitzroy road, Exeter, Devon, EX1 3 PB, UK, (http://www.metoffice.gov.uk)
HadGEM2-ES	192	144	
inmcm4	192	144	INM (Institute for Numerical Mathematics, Moscow, Russia)
IPSL-CM5A-LR	96	96	IPSL (Institut Pierre Simon Laplace, Paris, France)
IPSL-CM5A-MR	144	143	
MIROC5	256	128	AORI (Atmosphere and Ocean Research Institute, the University of Tokyo, Chiba, Japan)
MPI-ESM-LR	192	96	Max Planck Institute for Meteorology
MRI-CGCM3	320	160	MRI (Meteorological Research Institute, Tsukuba, Japan)
MRI-ESM1	320	160	
NorESM1-M	144	96	Norwegian Climate Centre

N_{lon} and N_{lat} indicates the number of points in longitude and latitude, respectively.

degree of spatial homogeneity in central Chile (Montecinos *et al*., 2000). Following Garreaud *et al*. (2017), these common variations were tracked by considering annual rainfall accumulations in six stations between 32° and 37°S with nearly complete records from 1915 onwards (highlighted in Figure 1). For each station, the annual series of observed accumulation was divided by its climatological value (1980–2010). The regional precipitation index (RPI, Figure 2a) was then calculated every year as the median of the seven station values. RPI has a high correlation (r ~ 0.7) with individual precipitation time series almost everywhere in central Chile.

Given our focus on regional dry spells in central Chile, drought events are identified as those years in which RPI ≤ 80% (≥20% deficit in rainfall), a threshold often used for hydrological and agricultural applications. This simple identification agrees well with those based on more sophisticated indices (e.g., SPI or the Palmer Drought Severity Index; see Garreaud *et al*., 2017 for details). Between 1915 and 2009, 24 years were classified as regional droughts (about a fourth of the time) mostly composed by one to 3-year long events (Figure 2a).

The Central Chile MD stands out in the RPI time series as the uninterrupted sequence of dry years since 2010, with RPI ranging between 55 and 80% (Figure 2a). This 9-year drought is substantially longer than any other event in the 20th century, although it does not include extremely dry (RPI < 50%) years like 1924, 1968 or 1998. The histogram of mean RPI considering 9-year blocks further illustrates the extraordinary character of the MD in the observational period (Figure 2b). In a longer-term context, tree-ring-based precipitation reconstruction for central Chile reveals only two analogues of the ongoing MD during the last millennium (Garreaud *et al*., 2017). Precipitation deficits over 25% were observed in more than three-quarters of the stations along central Chile in every year conforming the MD, although the rainfall anomalies have some spatial variability as illustrated by the station-based maps for individual years (Figure 3). These data support the findings in Garreaud *et al*. (2017) regarding the more persistent and extraordinary character of the MD in the southern half of central Chile.

4 | OBSERVED LARGE-SCALE ANOMALIES

In this section, we use reanalysis and observed data to describe the large-scale circulation and attending SST pattern during the MD. Most analyses are performed using austral winter (MJJAS) mean anomaly fields from 2010 to 2018, calculated as departures from the 1980–2010 climatology. We also consider dry years occurring before 2010 (see Figure 2a) to provide a historical background. For both the MD and past droughts, the precipitation anomaly maps (Figures 4a,d) reveals that dry conditions in central Chile are the easternmost expression of a broad band of rainfall deficit across much of the subtropical southeast Pacific. Dry conditions extend across the subtropical Andes into central Argentina but with weaker amplitude. To the south of 45°S, there is a tendency for wet anomalies from the central Pacific to the south Atlantic. A narrow dry band over the equatorial Pacific—all the way from the maritime continent to the coast of South America—is very prominent in the historical drought composite but mostly absent in the MD mean. As

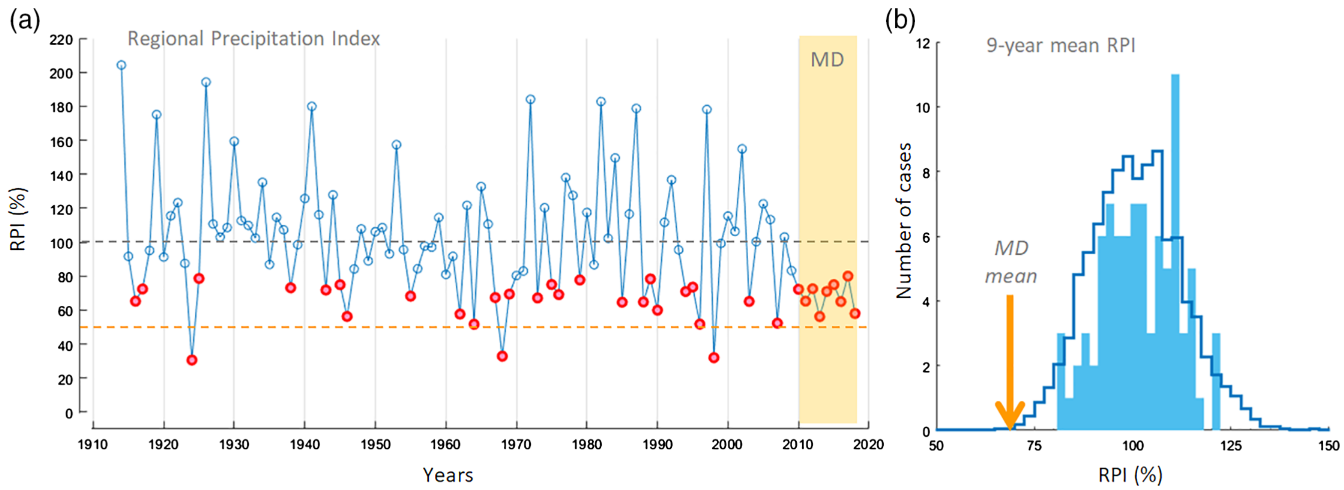

FIGURE 2 (a) Annual series of Central Chile regional precipitation index (RPI). Droughts, defined as years with RPI < 80%, are identified by the red circles. (b) Histogram of 9-year average of RPI for the period 1915–2009. The light blue bars show the observed frequency, considering a 9-year sliding window throughout the 1915–2009 record. The blue thick line is the distribution obtained from 5,000 randomly selected 9 years from the historical period. The orange arrow indicates the RPI averaged during the MD (2010–2018) [Colour figure can be viewed at wileyonlinelibrary.com]

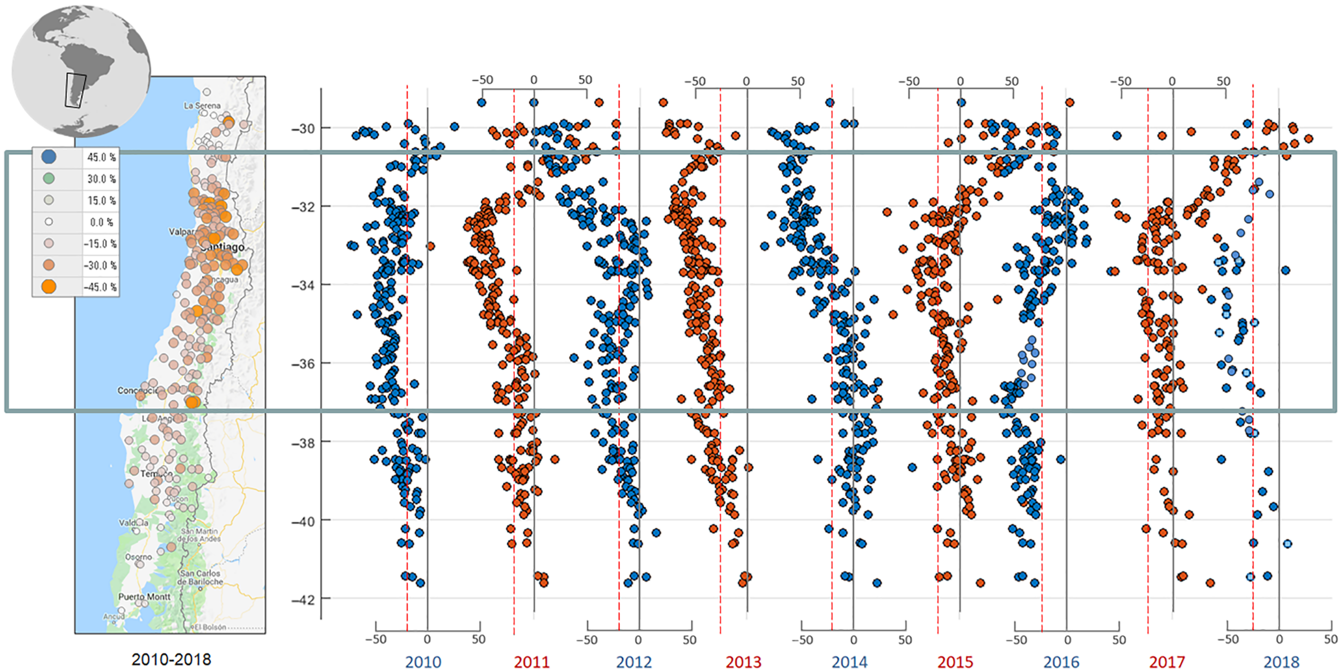

FIGURE 3 Station-based rainfall anomalies during the MD. In each station, the anomalies are calculated as the annual deficit (observed minus climatology values) divided by the climatology value (precipitation average 1980–2010). The map in the left shows the rainfall anomalies for the full period (2010–2018). The graphs show the anomalies for each year and station, sorted according to their latitude. The thick box encompasses Central Chile [Colour figure can be viewed at wileyonlinelibrary.com]

we describe later, this difference is connected with the varying impact of ENSO on central Chile hydroclimate.

4.1 | Circulation pattern and SAM impact

The composite map of 500 hPa geopotential height (Z500) anomalies during dry winters (Figure 4b) provides a dynamical perspective on central Chile historical droughts. Of particular relevance is a dipole of positive anomalies across the subtropical Pacific and negative anomalies at mid-latitudes. Such dipole, strongly related to ENSO variability, has been referred to as South Pacific Oscillation (SPO) and emerge as the leading mode of a Principal Component Analysis of the pressure field over this ocean basin (You and Furtado, 2017).

The South Pacific dipole is very prominent in the MD composite (Figure 4e) and evident every winter during this period, although the centres of the pressure anomalies exhibit some variability in their position and intensity (Figure S1). In average during the MD, the positive anomalies further extend over the tropical Pacific and the negative anomalies are very deep over the Amundsen–Bellinhausen Sea (ABS). The positive anomalies in the subtropics drive tropospheric-deep easterly wind anomalies over much of central Chile, a key factor behind regional dry conditions (Montecinos *et al.*, 2011; Garreaud *et al.*, 2013). Weaker westerlies associate with suppressed baroclinic instability and less frequent weather fronts reaching this region (Garreaud, 2007; Solman and Menéndez, 2002; see also Figure S2a). Reduced westerlies also weaken moisture transport from the Pacific (Campos *et al.*, 2018) and orographic precipitation forced by the Andes range (Falvey and Garreaud, 2007). By the contrary, enhanced transient activity—and hence precipitation—occurs over the tip of the continent and the Drake's passage, immediately downstream of the anomalous low over the ABS (Figure S2a).

The strength of the geopotential height dipole over the southeast Pacific can be gauged by the difference in Z500 between a subtropical box (centred at 30°S–110°W) and a mid-latitude box (centred at 65°S–90°W). Figure 5 shows the scatter plot between the winter mean height difference and central Chile rainfall anomalies (RPI) for the period 1948–2018. Consistent with the previous discussion, there is a negative relationship between both variables with a correlation coefficient of −0.6. The strength of the dipole has been consistently high from 2010 onwards resulting in a MD-average about 20% larger than the historical mean (Figure 5). The winter mean series of Z500 used to calculate the strength of the dipole over the South Pacific are shown in Figure 6. Both series exhibit substantial year-to-year variability, caused by either internal dynamics or remotely forced by SST anomalies in the equatorial Pacific. Superimposed on that variability there are negative/positive trends in Z500 in the mid-

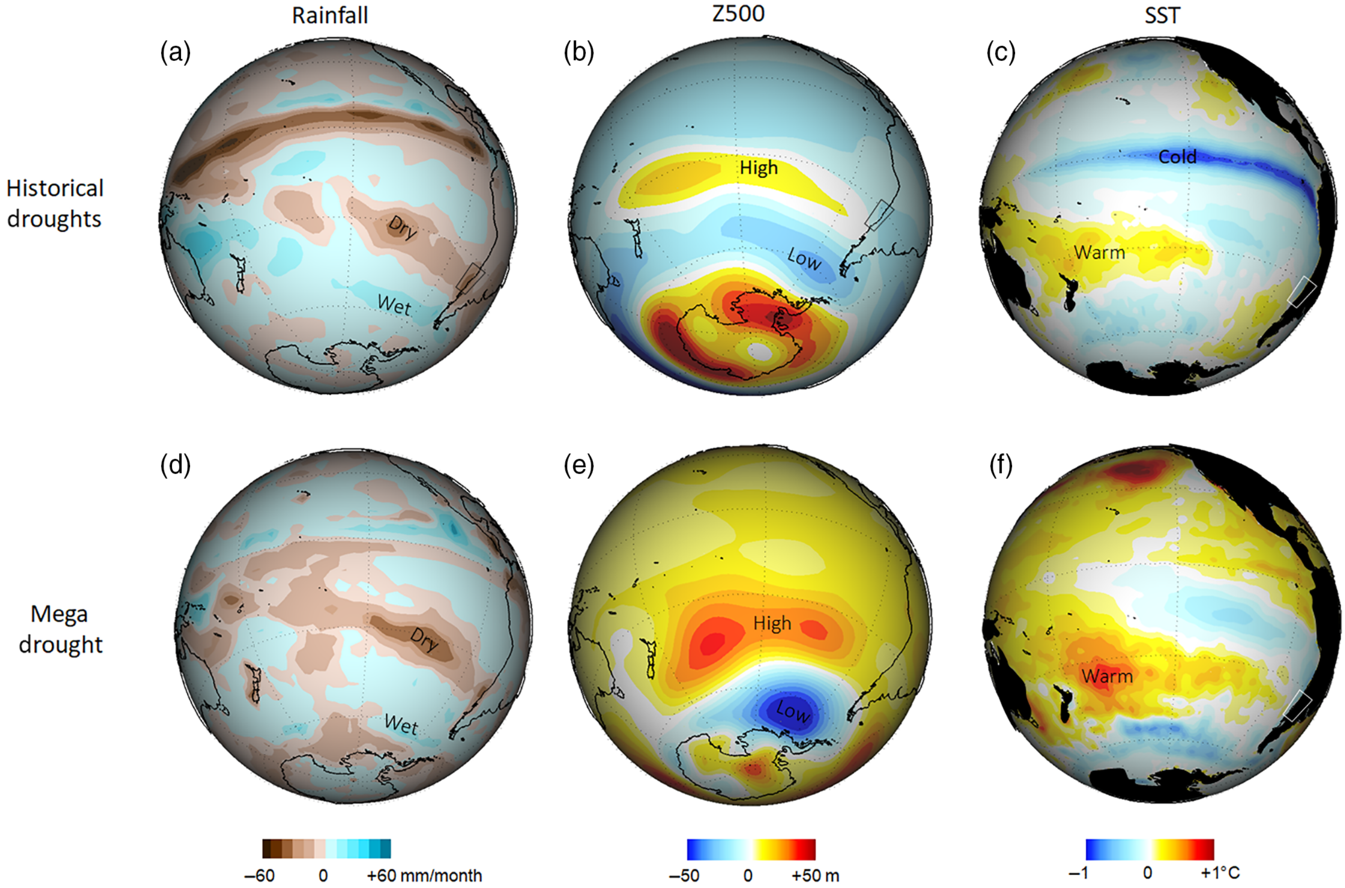

FIGURE 4 Composite anomalies (departures from de 1980–2010 mean) of austral winter (May–September) precipitation (GPCP, 1979 onwards), 500 hPa geopotential height (NNR; 1948 onwards) and sea surface temperature (ER-SST until 1980 and OI-SST from 1981 onwards). Upper panels: Historical droughts (identified in Figure 2a). Lower panels: MD period (2010–2018) [Colour figure can be viewed at wileyonlinelibrary.com]

latitude/subtropical box, evident since the 1970s and statistically significant at the 1% level. These opposing trends result in a southeast Pacific Z500 dipole strengthening of ~20 m/decade between 1980 and 2018. The magnitude of this trend is substantial and accounts for one-third of the dipole anomaly observed in average between 2010 and 2018.

The positive trend in mid-level geopotential height over subtropical latitudes can be linked to the overall tropospheric warming during the last decades (e.g., Sherwood *et al.*, 2008). The negative height trend over the ABS during wintertime is more puzzling. Only weak trends were found in that season in the last part of the 20th century (Fogt *et al.*, 2012), but after year 2000 reanalysis data shows a marked drop (R. Fogt 2018, personal communication). The SAM pattern strongly projects upon the strength of the height anomaly dipole ($r \approx 0.75$; see also Fogt *et al.*, 2012), so part of the augmented meridional gradient over the south Pacific arises from the SAM trend towards its positive polarity (Marshall, 2003; Jones *et al.*, 2016). In turn, the SAM trend has been largely attributed to stratospheric O_3 depletion and increased GHG concentration (Arblaster and Meehl, 2006; Eyring *et al.*, 2013; Gillett *et al.*, 2013), thus, supporting the hypothesis that anthropogenic forcing have played a relevant role on the drying tendencies and on the maintenance of MD in central Chile (Boisier *et al.*, 2016).

4.2 | Influence of ENSO

ENSO impacts on the hydroclimate of central Chile in the form of a warm/wet - cold/dry relationship by exciting the South Pacific dipole (e.g., Aceituno, 1988; Rutllant and Fuenzalida, 1991; Montecinos and Aceituno, 2003). Indeed, the composite map of SST anomalies during historical droughts exhibits a marked cooling across much of equatorial Pacific, weaker cool anomalies over the subtropical southeast Pacific, and a horse-shoe pattern of warmer anomalies rooted in the tropical western Pacific (Figure 4c). All these features conform the well-known pattern of SST anomalies during a La Niña event (e.g., Rasmusson and Carpenter, 1982; Capotondi *et al.*,

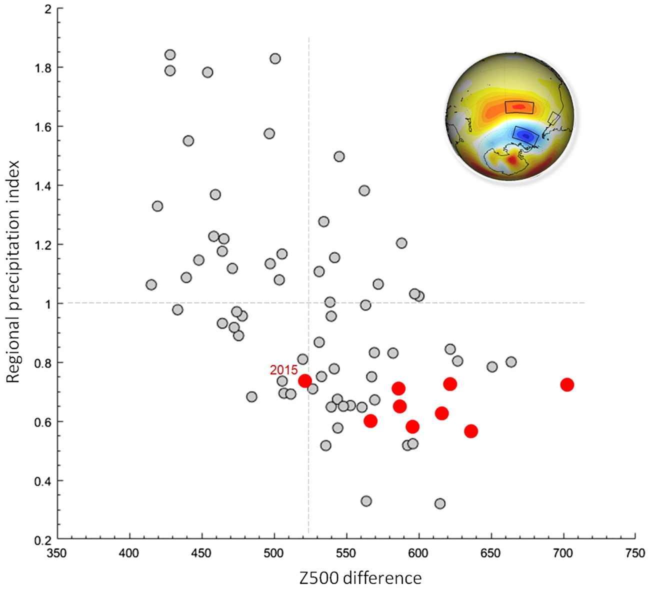

FIGURE 5 Scatter plot between the Central Chile precipitation index (RPI) and the difference of winter mean 500 hPa geopotential height between a box over the subtropical Southeast Pacific (30°–40°S; 140°–110°W) and a box over the Amundsen Bellinhausen Sea (60°–70°S; 110°–80°W). Data from 1948–2018. The years forming the MD are indicated in red [Colour figure can be viewed at wileyonlinelibrary.com]

2015). The scatter plot between winter values of Niño3.4 and central Chile rainfall anomalies (Figure 7), however, shows that the statistical relation is moderate (r ~ +0.6) and that during ENSO neutral winters rainfall is distributed over a wide range.

The SST anomaly field during the MD shares some features with its historical counterpart (Figures 4c,f), namely, the weak cold anomalies over most of the subtropical SE Pacific and the horse-shoe pattern of warm anomalies rooted in the maritime continent. A remarkable difference, however, is the lack of significant cold—La Niña-like—anomalies along the equatorial Pacific during the MD, even if the winter 2015 (when a strong ENSO was developing) is excluded. Considering a threshold of ±0.5°C of the winter mean Nino3.4 index for El Niño/La Niña classification, only 2010 qualified as La Niña, ENSO-neutral conditions prevailed from 2011 to 2014, 2015 qualified as a strong El Niño, and ENSO-neutral winters return in 2016–2018 (Figure 7). This suggests that ENSO had little influence in the maintenance of the rainfall deficit in central Chile during the MD period.

Moreover, although dry winters under ENSO-neutral conditions are not uncommon, a 6-year drought chain seems unlikely. To assess the likelihood of such dry sequence we made 5,000 random extractions of 6 ENSO-neutral years (without replacement) from the historical RPI time series (1920–2009). The probability of having a 6-year sample with a mean rainfall deficit ~25% is less than 2.5%, and the probability of having such deficit in each individual year (as the current MD) is 0.5% or less, indicative of the influence of other modes in sustaining the long drought in central Chile.

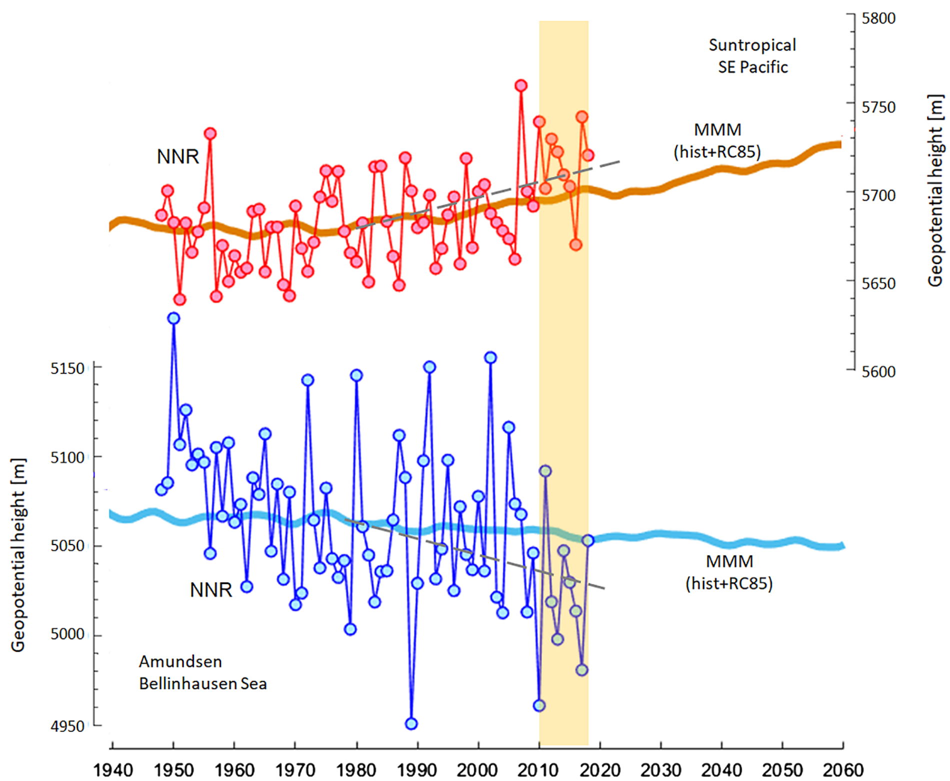

FIGURE 6 The lines with circles are the time series of the observed (NNR) winter mean (May–September) 500 geopotential height at a box over the subtropical Southeast Pacific (30°–40°S; 140°–110°W) and a box over the Amundsen Bellinhausen Sea (60°–70°S; 110°–80°W). The MD period is highlighted. The orange (light blue) thick line is the CMIP5 multi model mean 500 geopotential height in the subtropical (mid-latitudes) box considering the historical runs (1940–2005) and the RCP8.5 runs (2006 onwards). Each simulated series (from 43 fully coupled models) were previously low-pass filtered (5-year moving average) and adjusted so their 1960–1990 mean coincided with the observed (NNR) mean for that period [Colour figure can be viewed at wileyonlinelibrary.com]

4.3 | Influence of ocean-sourced decadal variability

Rainfall variability in central Chile has also been related to low frequency phenomena, particularly to the Pacific Decadal Oscillation. Consistent with the ENSO-like structure of the PDO and attending teleconnections in the SH (Garreaud and Battisti, 1999), its cold (warm) phase tends to produce extended periods that are in average drier (wetter) than the long term mean in central Chile (Garreaud *et al.*, 2009; Masiokas *et al.*, 2010; Muñoz *et al.*, 2016; González-Reyes *et al.*, 2017). This relation is summarized in Figure 8 by the scatter plot between multi-year average of the PDO index and the corresponding RPI in central Chile. The periods were selected as sequences of years in which the PDO was predominantly in its warm or cold phase. The statistical relationship is modest ($r \approx 0.4$), but we acknowledge that such analysis is based on only a few PDO multi-year blocks.

After the regime shift in the mid 1970s (Jacques-Coper and Garreaud, 2014), the PDO remained in its positive phase during the next three decades but for brief negative excursions in 1990 and 1999–2002. Around 2007, the PDO index became negative until the end of 2014, when it flipped again to its positive phase. The mostly positive PDO indices from 1980s to 1990s and mostly negative indices after 2005 resulted in a negative trend year round during the last three decades (Clem and Fogt, 2015). During the MD period, the PDO index has exhibited both polarities during, with a multi-year median of −0.15 and a mean of +0.1. Considering the PDO-rainfall relationship from the historical record (Figure 8) one would expect near average rainfall conditions for the 2010–2018 period. Even if we restrict the analysis to 2010–2014 (when the mean PDO was −0.45) the observed rainfall deficit (30%) is well below the PDO-congruent range (15–22%). Considering the uncertainty in the PDO-rainfall relationship, this analysis suggests that the mostly negative PDO phase during the last decade has contributed to the dry conditions in central Chile but it is insufficient to explain the full intensity and persistence of the current Mega Drought. Similarly, Boisier *et al.* (2016) found a substantial but partial role of the PDO negative trend in the observed drying trend over the southeast Pacific (including central Chile) during the last few decades.

In describing the composite SST anomalies during the MD, the warming of the subtropical southwest Pacific (SSWP) stands out (>1°C just northeast of New Zealand, Figure 4f). Warmer than normal conditions in that region also appears in the historical drought composite -in connection with La Niña conditions- but with much lesser magnitude (<0.3°C). The marked anomalies at the surface of the SSWP during the last decade are partially explained by a warming trend since the late 1980s (Figure 9a,b; see also Saurral *et al.*, 2018) that also involves the deep ocean (Volkov *et al.*, 2017). In turn, part of the surface warming is related to the shift in the PDO from its positive to negative polarity over the past decades (England *et al.*, 2014; Saurral *et al.*, 2018). The impact of the SSWP warming upon central Chile rainfall deficit is explored in Section 5.1.

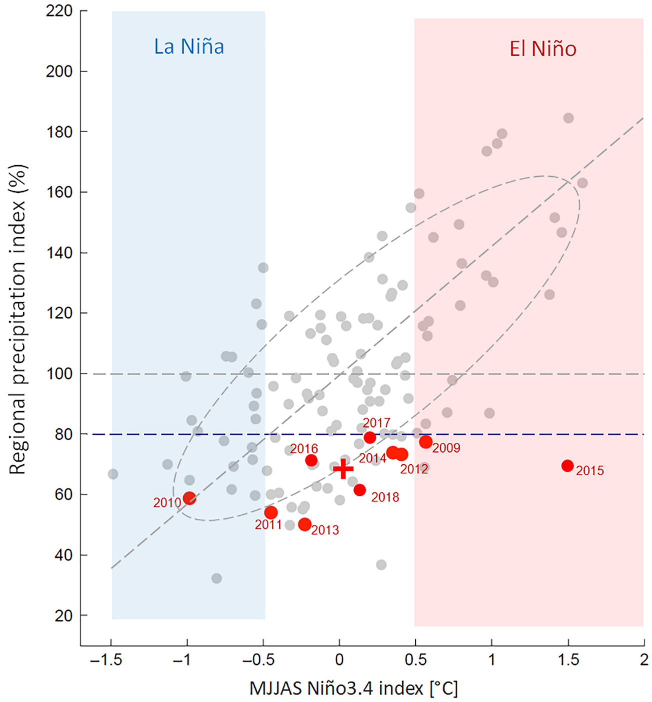

FIGURE 7 Scatter plot between the winter (MJJAS) average of the Niño3.4 index and the Central Chile precipitation index (RPI). Data from 1915 to 2018. The years forming the MD are indicated in red. The Niño3.4 index is the area average SST anomaly in the region 5°S–5°N and 170°–120°W [Colour figure can be viewed at wileyonlinelibrary.com]

5 | INSIGHTS FROM GLOBAL CLIMATE MODELS

The observational evidence presented in the previous sections has revealed that the exceptional length of the ongoing drought in central Chile results from the uninterrupted reiteration of a large-scale circulation pattern disfavouring the passage of frontal systems over central Chile. This pattern is characterized by tropospheric-deep positive pressure anomalies over the central-eastern subtropical Pacific and negative anomalies over the Amundsen-Bellinhausen Sea. Both natural (e.g., the cold PDO phase) and anthropogenic forcing (through the positive phase of SAM) can produce such pattern and appear to be acting during the central Chile MD. In this section, we use three families of global simulations—described in Section 2.1 and 2.2—to gauge the importance of these factors.

5.1 | Ocean forcing

The left panels of Figure 10 show the CAM5 AMIP-ORF (i.e., observed SST and radiative forcing) ensemble mean anomalies of Z500 and precipitation averaged during the MD (austral winter of 2010–2017 given the data availability). The ensemble mean replicates the key dynamical pattern sustaining dry conditions in central Chile: negative anomalies over the ABS and positive anomalies over the subtropical Pacific (Figure 4e). Consistently, the simulated area of negative rainfall anomalies over the west coast of South America and adjacent ocean is in good agreement with its observational counterpart (Figure 4d). The MD mean pattern of Z500 and rainfall anomalies is also found in individual winters. The amplitude of the CAM5 ensemble mean Z500 anomalies at the mid-latitude and subtropical sectors of the south Pacific are about two-thirds of the observed values. Likewise, the MD-averaged ensemble mean rainfall anomalies in Central Chile reaches about $-17 \pm 5\%$, below the observed value of -30% (Figure 10). Nonetheless, five members (out of 40) show an MD-average rainfall deficit that reach and even exceed the observed value as summarized by the box plot in Figure 11. Similar findings emerge when using the AMIP ensemble runs with SPEEDY.

These AMIP results strongly suggest that the protracted Central Chile MD was substantially driven by global SST anomalies, while internal atmospheric variability would enhance its severity. Such inference is somewhat surprising given the mostly ENSO-neutral conditions during the MD but consistent with the mostly negative PDO phase during this period. The outstanding question is then, from where in the SH extratropical oceans is emerging the atmospheric forcing of the dry conditions in central Chile? A plausible candidate is the subtropical southwest Pacific (SSWP, 30–40°S, 190–210°W), a region that has exhibited a substantial warm anomaly throughout the MD period (Figure 4f). Such surface warming may shift the tropical convection or lead to anomalous deep convection locally (Figure 2b), perturbing the tropospheric flow throughout Rossby wave generation (e.g., Hoskins and Karoly, 1981; Hoskins and Ambrizzi, 1993; Mo and Higgins, 1998). This

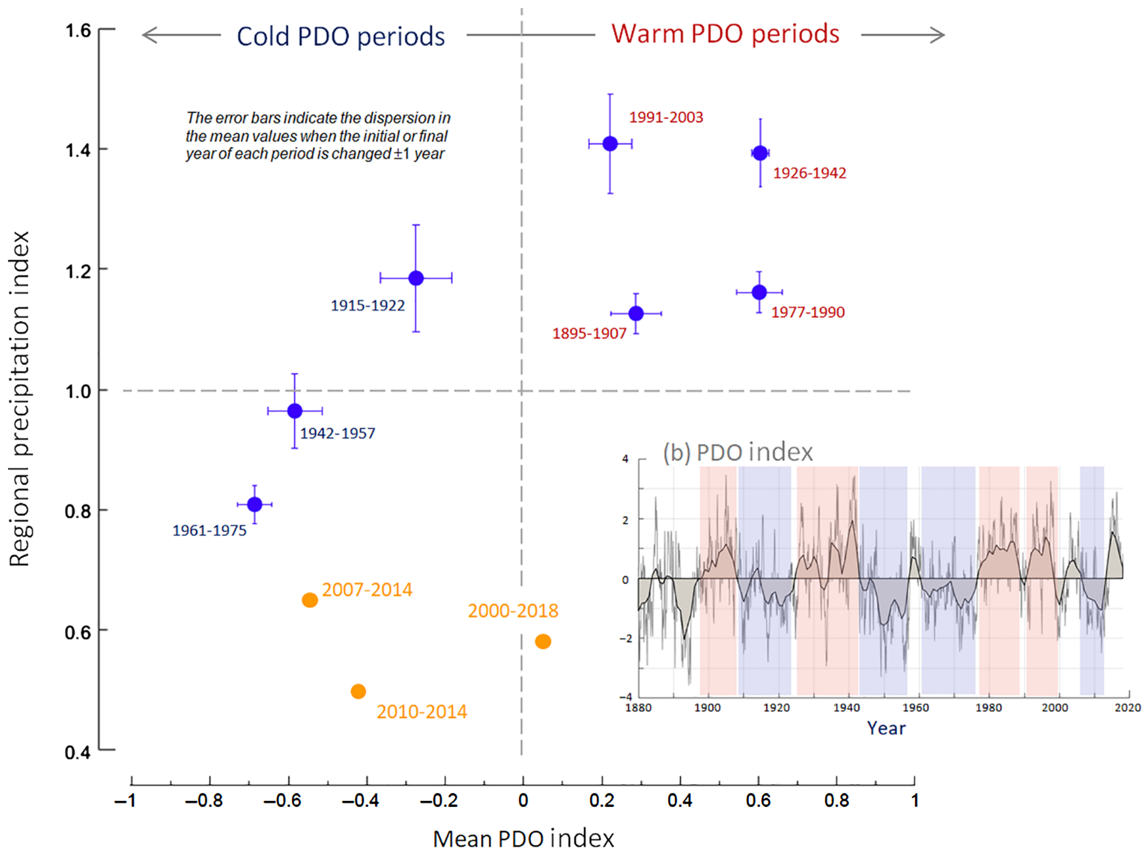

FIGURE 8 Scatter plot between multi-year winter (MJJAS) average of the PDO index and the concurrent Central Chile precipitation index (RPI) average. The periods were selected as sequences of years in which the PDO was predominantly in its cold or warm phase (see inset with the PDO time series). The MD period in the PDO-RPI space is highlighted. The PDO index is defined as the leading principal component of North Pacific monthly sea surface temperature variability (poleward of 20°N); monthly values obtained from http://research.jisao.washington.edu/pdo/ [Colour figure can be viewed at wileyonlinelibrary.com]

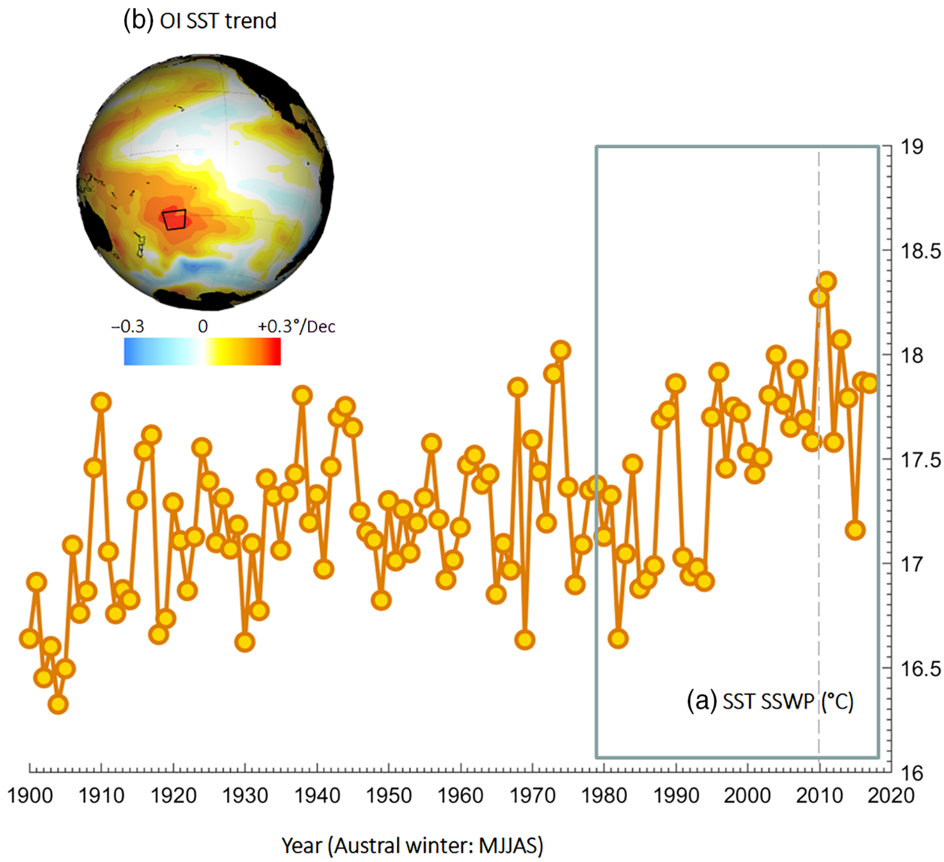

FIGURE 9 (a) Time series of winter (MJJAS) mean of sea surface temperature (NOAA ER-SST) over the subtropical Southwest Pacific (SSWP, 30°–40°S, 190°–210°W). (b) Trends in winter mean SST (from NOAA OI-SST) over the Pacific from 1981 to 2018 [Colour figure can be viewed at wileyonlinelibrary.com]

perturbation eventually reaches South America in a way that is favourable to dry conditions in Chile.

To test this hypothesis, we conducted an ad-hoc numerical experiment using SPEEDY (Section 2.3). We first produced a 50-member ensemble of 30-year SPEEDY simulations using climatological mean SST (CTR simulations). The ensemble mean of wintertime precipitation, SLP and Z500 are shown in Figure 12a and reproduce well the key elements of the large scale circulation. We then repeated these simulations (50 runs in each case) but adding an SST perturbation of {+0.5, +1.0, +1.5, +2.0, +2.5}°C in the SSWP domain. The difference between SSWP+2.5 and CTR ensembles in precipitation, SLP and Z500 are shown in Figures 12b,c. The warming of the SSWP produces a local, baroclinic response that features a drop in SLP, enhanced precipitation and increased Z500. There is also a barotropic response downstream of the region of warming that include negative anomalies at higher latitudes, centred over the Antarctic Peninsula, and positive anomalies at subtropical latitudes, largest over the west coast of South America. This pattern strongly projects upon the dipole that favour a reduction of precipitation in central Chile (cf. Figures 4 and 12). Indeed, the SSWP+2.5 wintertime precipitation in central Chile is about 25% lower than its CTR counterpart, a significant difference considering the role of internal variability within the various ensemble members (Figure 12d). Sensitivity simulations with intermediate SST perturbations indicate a mostly linear response of central Chile precipitation deficit to the warming over subtropical southwest Pacific.

Specific details on the mechanism linking the SSWP warming and central Chile drought warrant further investigation. As a first approximation, Figure 13 show the streamfunction anomalies for the 0.2101 sigma-level from NCEP NCAR reanalysis. The streamfunction anomalies are calculated as the average of the anomalies for individual months from May to September in the period from 2010 to 2017. The period between 1980 and 2010 is used as a base for climatologies. The W-vector shows the horizontal wave activity flux (Takaya and Nakamura, 2001) corresponding to this stream function anomaly field. W-vector has been previously used to diagnose Rossby wave propagation from the tropical Pacific into South America in time scales from daily to seasonal (Montecinos *et al.*, 2011; Rondanelli *et al.*, 2019). Anticyclonic and cyclonic anomalies in the upper atmosphere are located nearly in the same position as the 500 hPa geopotential high and low anomalies previously identified as a dipole. The anomalies have a barotropic equivalent vertical structure. Wave activity flows from the maximum heating region (indicated with a rectangle) and into the polar upper level cyclonic anomaly. The maximum mid-latitude upper level anticyclonic anomaly also seems to

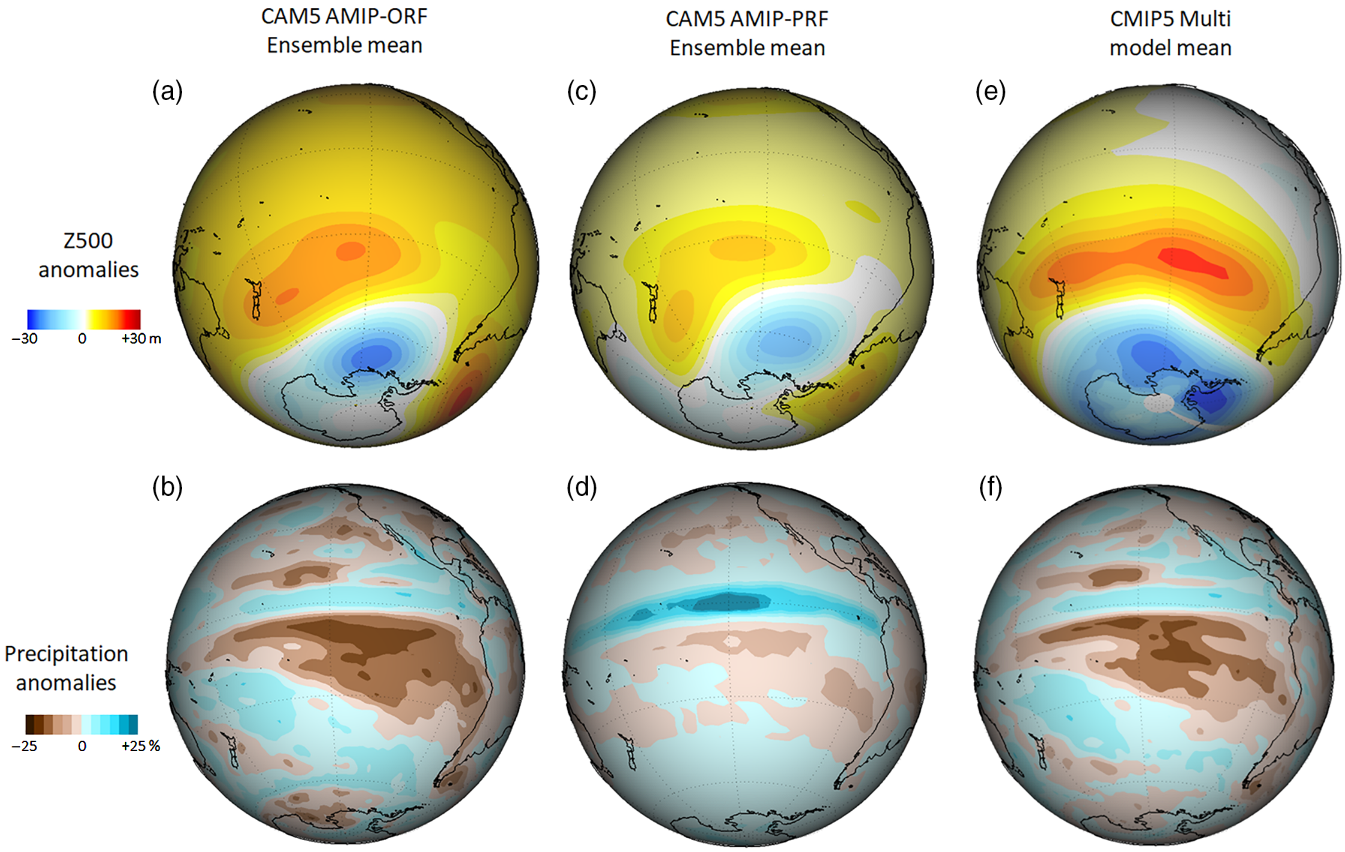

FIGURE 10 Mean anomalies during the MD of 500 hPa geopotential height (top panels) and precipitation (lower panels) from the (a,b) CAM5 simulations using observed SST, SIC and radiative forcing (AMIP-ORF) and (c,d) CAM5 simulations using observed SST, SIC and past radiative forcing (AMIP-PRF). The ensemble-mean (40 members) was first calculated for each winter (MJJAS). We then calculated the anomaly by subtracting the ensemble-mean climatology (1970–2010) and finally we calculated the average over the period 2010–2017. Panels (e,f): Difference between present-day (2010–2020) minus recent past (1970–2000) in winter (MJJAS) fields on the basis of the multi-model mean from 43 CMIP5 fully-coupled simulations [Colour figure can be viewed at wileyonlinelibrary.com]

contribute with wave activity towards the polar low. Since W-vectors are nearly parallel to a quasi-stationary Rossby wave at each point, poleward wave activity flowing from the surface heating region seems to be consistent with a low wave number quasistationary Rossby wave. A low wavenumber propagation is also consistent with the horizontal scale of the anomalies, cyclonic and anticyclonic anomalies covering about 90° longitude, translating into horizontal wavenumber 2. At around 75°S and near the Antarctic Peninsula, wave activity shifts equatorward and into the Atlantic.

5.2 | Anthropogenic forcing

We now return to the CAM5 AMIP simulations but now considering those integration using 1880s radiative forcing (CAM5 AMIP-PRF). The overall structure of the ensemble mean Z500 and precipitation anomalies during the MD also agree well with the observations but the amplitude of key features is reduced (Figure 10c,d). Of particular relevance, the ensemble mean rainfall anomalies in central Chile is $-8 \pm 4\%$ and none of the members produce a deficit as large as observed (Figure 11). Thus, while both CAM5 AMIP-ORF and AMIP-PRF simulations reveal an important ocean-forced component of this drought, this forcing seems to produce an event with a severity close to the observations only when the model incorporates the current—anthropogenic—atmospheric levels of GHG, O_3 and aerosols.

The differences between CAM5 AMIP-PRF and AMIP-ORF may be interpreted as an indication of the anthropogenic interference in sustaining the Central Chile MD. A more direct evidence is provided by the fully coupled simulations (CMIP5) including all climate forcing (Section 2.3). The rightmost panels of Figure 10 shows the multi-model mean difference between present (2010–2020) and recent past (1970–2000) global Z500 and precipitation. Note that to increase the signal to noise ratio, the averaging period (2010–2020) for these simulations is slightly larger than the observed MD interval. As noted in previous studies

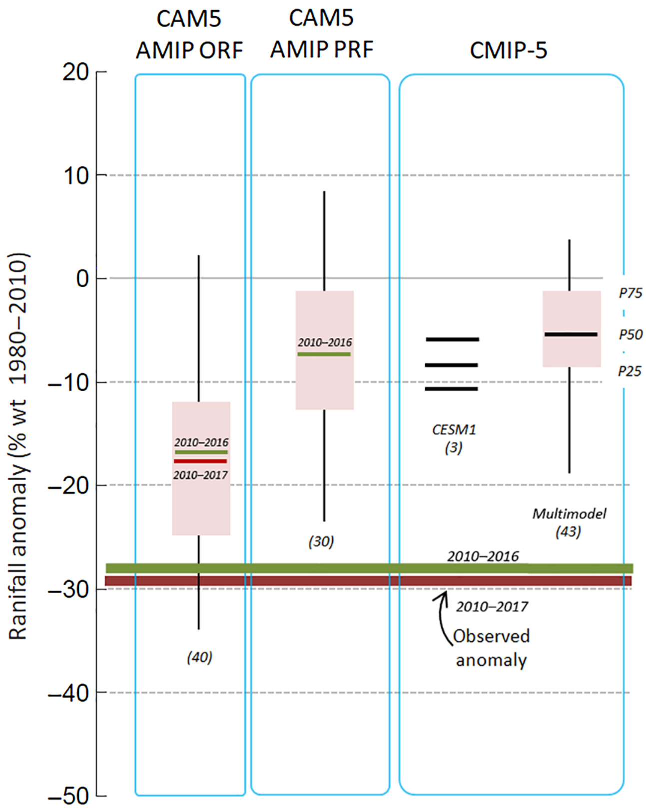

FIGURE 11 Summary of the Central Chile MD mean rainfall deficit from different simulations. The winter (MJJAS) rainfall anomaly over the region 32.5–37.5°S, 74–70°W was calculated for every year and family of simulations. We then calculated the yearly anomalies by subtracting the climatology (1970–2010), that were averaged during the MD period. Each family of simulations include multiple runs (for CAM5) or multiple models (form CMIP5), that allows to construct box plots showing the median value (colour line), interquartile range (pink box) and the [5%,95%] range (black vertical line). The observed (station based) MD rainfall deficit is also indicated. The red and green lines correspond to the average during 2010–2017 and 2010–2016, respectively [Colour figure can be viewed at wileyonlinelibrary.com]

(e.g., Fyfe *et al.*, 1999; Arblaster *et al.*, 2011; Gillett and Fyfe, 2013; Boisier *et al.*, 2016), the anthropogenic forcing leads to a marked Southern Annular Mode pattern in its positive polarity, with negative height anomalies over the Antarctic periphery and positive anomalies at lower latitudes. The Z500 anomalies found in the 2010–2020 period are part of gradual trends over the subtropical Pacific and ABS of the same sign of their observed counterparts, evident in the multi-model mean time series of 500 hPa geopotential height in the boxes defined before (Figure 6). Notably, the positive height trend since the late 1970s over the subtropics is quite comparable with its observed counterpart, but the simulated height decline over the ABS is weaker than the reanalysis value.

The positive SAM polarity shown by CMIP5 models for the present decade (Figure 10e) strongly projects upon the dynamical pattern that favours dry conditions in central Chile (Section 4.1). Indeed, the multi-model mean precipitation anomalies exhibit a dry band over the subtropical southeast Pacific reaching central Chile (Figure 10d) resembling the observations. The CMIP5 simulations also predicts an overall increase in SST but less marked along the west coast of South America than in the rest of the Pacific. A more quantitative view of the climate change impacts on central Chile in present time can be obtained from the distribution of rainfall anomalies from the 26 CMIP5 models for the period 2010–2020 (Figure 11). The multi-model mean deficit for central Chile is $-6 \pm 3\%$, so anthropogenic-induced precipitation changes appears to explain about a quarter of the observed rainfall anomaly in this region. Note that the mean rainfall deficit "predicted" by the CMIP5 simulations is similar to the RPF value (although the last number comes from just one model). To test its significance we employed the historical simulations (1850–2005) of the same 26 models. To avoid a major influence of the anthropogenic forcing we only consider the period 1900–1950 and from there we randomly selected ten 10-year periods. In each of those periods, we calculated the multi-model mean central Chile rainfall anomalies, and then we obtained the ensemble mean rainfall statistics. The multi-model mean over this synthetic "unperturbed" period is close to zero (+0.3%) with a SD of 2.2%. On the basis of these values, we posit that the predicted rainfall anomalies ($-6 \pm 3\%$) for the MD are significant at the 95% confidence level against the null hypothesis of no anthropogenic driven drying and represents about a quarter of the total (observed) signal (~25% rainfall deficit). Such level of the human contribution was also reported by Boisier *et al.* (2016) and is much larger than its counterpart in the 2011–2014 California droughts (e.g., Seager *et al.*, 2015). Yet, the diagnosed rainfall anomalies vary substantially among the models, probably because of the short difference in time between the present (2010–2020) and the past (1970–2000) periods. In such case, internal variability within each model can be stronger than the forced signal (Deser *et al.*, 2012). We also verified that among the CMIP5 simulations those predicting the largest drying in central Chile (15–20% rainfall deficit) feature an SST anomaly pattern resembling the observed in the last decade (warm in the west Pacific, cool in the far east; not shown). This SST pattern emerged in those simulations given its own internal, coupled variability and stress the hypothesis that direct (atmospheric-circulation) anthropogenic forcing can cause a drought as observed only if coupled with a La-Niña like SST pattern of enough longevity (i.e., during the cold phase of PDO).

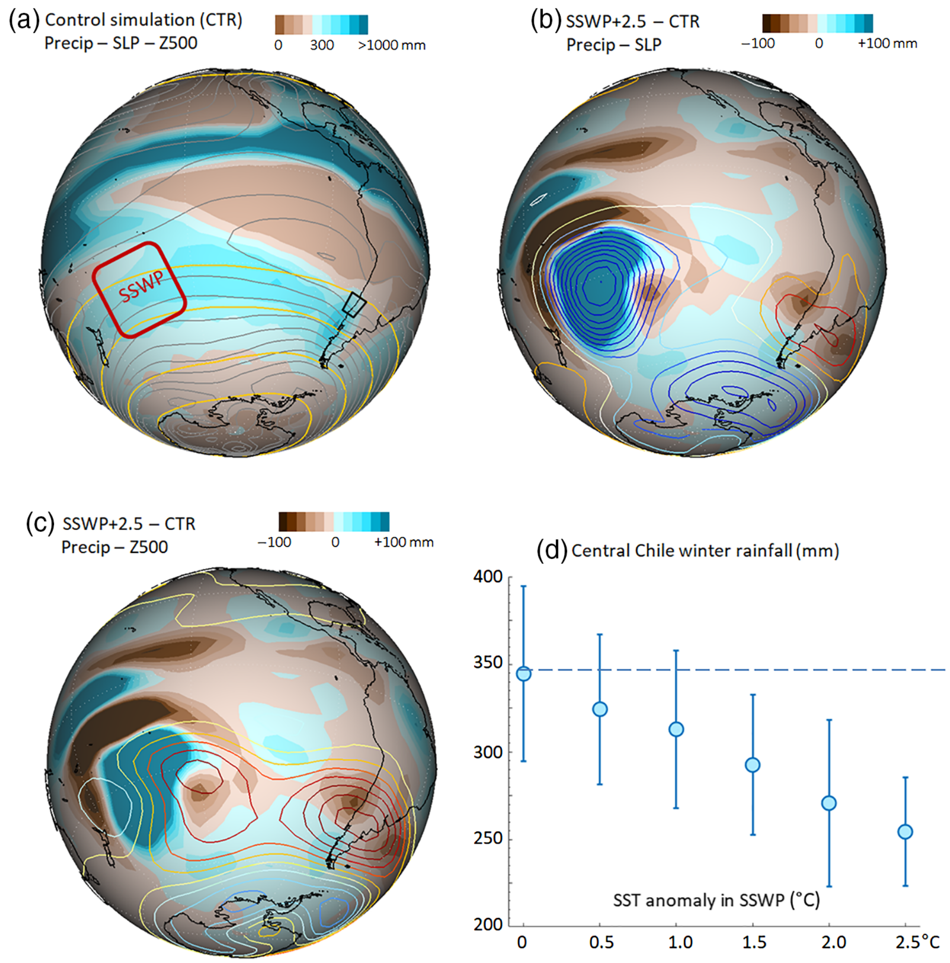

FIGURE 12 (a) Ensemble mean (50 members), multi-year mean of winter precipitation (colour), sea level pressure (SLP, grey contours every 3 hPa) and 500 hPa geopotential height (Z500, yellow contours at 5250, 5400 and 5,600 m) from a 30-year long SPEEDY control simulation (CTR) forced by climatological monthly mean SST. (b) Differences of ensemble mean precipitation (colours) and SLP (contours, every 0.15 hPa) between SSWP+2.5 minus CTR simulations. SSWP+2.5 is identical to CTR but for a permanent warm anomaly of +2.5°C in the subtropical Southwest Pacific (30–40°S, 190–210°W). (c) Differences of ensemble mean precipitation (colours) and Z500 (contours, every 7.5 m) between SSWP+2.5 minus CTR simulations. (d) Multi-year winter mean precipitation over Central Chile (32.5–37.5°S, 74–70°W) for the climatological SPEEDY simulations. The circle is the ensemble mean and the vertical lines indicate the interquartile range. The horizontal axis indicate the SST anomaly imposed in the SSWP region [Colour figure can be viewed at wileyonlinelibrary.com]

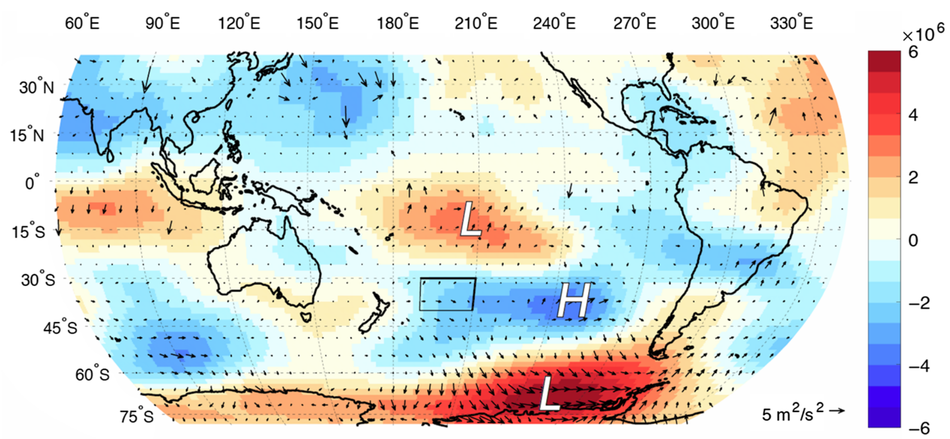

FIGURE 13 NNR streamfunction anomalies (colours in m2/s) and W vectors (m2/s2). Both fields are calculated from monthly anomalies in the period 2010–2017 for the months from may to September. W-vectors after Takaya and Nakamura (2001). Climatologies are with respect to the period 1980 to 2010. H and L indicate the center of anticyclonic and cyclonic anomalies, respectively. The black rectangle shows the subtropical Southwest Pacific (SSWP) region [Colour figure can be viewed at wileyonlinelibrary.com]

6 | CONCLUDING REMARKS

The central Chile MD(2010–2018) has been the longest sequence of dry years during the observational period (1914 onwards) and has few (if any) analogues in the last millennia, perhaps heralding the dry conditions projected for this region during the rest of the 21st century (Boisier *et al*., 2018; Bozkurt *et al*., 2018). Its detrimental effects have been observed in water availability, vegetation and forest fires (Garreaud *et al*., 2017). In this work, we have used observational datasets to document regional- and large-scale features of the MD, emphasizing those aspects that differ from previous dry events. We also took advantage of atmospheric-only and fully coupled GCMs to gauge the role of natural variability and anthropogenic forcing in sustained such extended drought. Our main findings are as follow:

- The exceptional length of the MD results from an uninterrupted reiteration of a large-scale circulation pattern during austral winter hindering the passage of extratropical storms over central Chile. This pattern is characterized by tropospheric-deep positive pressure (anticyclonic) anomalies over the central-eastern subtropical Pacific and negative pressure (cyclonic) anomalies over the Amundsen-Bellingshausen Sea. The strength of this dipole has been substantially above the long-term mean during the MD.
- Historically, ENSO is a major modulator of the south Pacific dipole, producing low (high) pressure anomalies over the ABS (subtropical latitudes) during La Niña years. Unlike historical droughts, however, the ongoing dry period has occurred mostly under ENSO-neutral conditions, except for the winters of 2010 (La Niña) and 2015 (strong El Niño). This has resulted in a substantial decrease in the ability to foresee central Chile hydroclimate based on ENSO predictions (J. Vicencio, personal communication).
- Nonetheless, atmospheric-only GCM simulations forced with observed global SST and present-day radiative forcing (AMIP ensembles) replicates the south Pacific dipole and the area of negative rainfall anomalies during the MD. The simulated precipitation deficit is 1/2 to 2/3 of the observed values, and much smaller if the radiative forcing is set to pre-industrial levels. These results confirm that the protracted Central Chile MD is largely driven by global SST anomalies of the last decades under the current (anthropogenic) levels of greenhouse gases and stratospheric ozone.
- Further numerical experiments suggest that most of the atmospheric forcing emanates from the subtropical southwest Pacific (SSWP), although specific details of such link deserve further investigation. This area has experienced a marked sea surface warming over the last 20 years, with mean anomalies over +1°C during the MD period. Such warming is capable to excite a Rossby waves response whose propagation lowers the pressure over the ABS and increases the pressure over western South America, projecting upon the pattern that lead to dry conditions in central Chile.
- The origin of the SSWP warming is unclear, but partially connected with the shift in the PDO from its positive to negative polarity over the past decades (e.g., Saurral *et al*., 2018). Yet, climate change projections also reveals substantial west–east asymmetries in the SST change across the south Pacific at subtropical latitudes, thus, contributing to the anomalous warming of the SSWP.
- The tendency of the Southern Annular Mode towards its positive polarity also contributes to strength of the dipole leading to rainfall deficit in central Chile. In turn, the SAM trend has been largely attributed to stratospheric O_3 depletion and increased GHG concentration (Arblaster and Meehl, 2006; Eyring *et al*., 2013; Gillett *et al*., 2013). Indeed, fully-coupled GCM forced by observed radiative forcing also produce a dry band over the subtropical southeast Pacific reaching central Chile, with a multi-model mean deficit of about 5% for the present decade relative to the recent past.
- A subset of CMIP5 simulations produce a rainfall deficit closer to the observed values and feature a La-Niña like SST anomaly pattern, stressing again the relevance of the ocean sourced forcing of the MD, that is currently enhanced by changes in atmospheric circulation driven by anthropogenic forcing.

In summary, both natural variability (PDO shift causing SSWP warming) and anthropogenic forcing (SAM trends towards its positive polarity) are at play in sustaining the Central Chile Mega Drought. While it is not possible to obtain an exact partitioning, the seemingly natural, ocean-forced component appears as dominant, accounting for at least half of the dry signal in central Chile. Given its origin in ocean–atmosphere variability, a reversal of its sign can be expected for the next decades, partially relieving the dry conditions afflicting central Chile. Nevertheless, the anthropogenic forcing is also important—about a quarter of the MD signal—and it will keep pushing Central Chile towards a dry condition during the rest of 21st century with an intensity that depend upon the emission scenario that humanity will follow.

ACKNOWLEDGEMENTS

This research emerged from the collaboration with many colleagues at the Center for Climate and Resilience Research (CR2, CONICYT/FONDAP/15110009) that also provided partial funding. R.G. also acknowledges for support by Fondecyt project 1170286. We thank two anonymous reviewers for constructive criticism and comments on the manuscript.

ORCID

René D. Garreaud https://orcid.org/0000-0002-7875-2443

REFERENCES

Aceituno, P. (1988) On the functioning of the southern oscillation in the south American sector. Part I: surface climate. *Monthly Weather Review*, 116, 505–524.

Adler, R.F., Huffman, G.J., Chang, A., Ferraro, R., Xie, P.-P., Janowiak, J., Rudolf, B., Schneider, U., Curtis, S. and Bolvin, D. (2003) The version-2 global precipitation climatology project

(GPCP) monthly precipitation analysis (1979–present). *Journal of Hydrometeorology*, 4, 1147–1167.

AghaKouchak, A., Cheng, L., Mazdiyasni, O. and Farahmand, A. (2014) Global warming and changes in risk of concurrent climate extremes: insights from the 2014 California drought. *Geophysical Research Letters*, 41, 8847–8852. https://doi.org/10.1002/2014GL062308.

Aldunce, P., Araya, D., Sapiains, R., Ramos, I., Lillo, G., Urquiza, A. and Garreaud, R. (2017) Local perception of drought impacts in a changing climate: the mega-drought in Central Chile. *Sustainability*, 9, 2053. https://doi.org/10.3390/su9112053.

Arblaster, J.M., Meehl, G.A. and Karoly, D.J. (2011) Future climate change in the southern hemisphere: competing effects of ozone and greenhouse gases. *Geophysical Research Letters*, 38(2), L02701. https://doi.org/10.1029/2010GL045384.

Arblaster, J.M. and Meehl, G.A. (2006) Contributions of external forcings to southern annular mode trends. *Journal of Climate*, 19, 2896–2905. https://doi.org/10.1175/JCLI3774.1.

Boisier, J.P., Rondanelli, R., Garreaud, R.D. and Muñoz, F. (2016) Anthropogenic and natural contributions to the Southeast Pacific precipitation decline and recent megadrought in Central Chile. *Geophysical Research Letters*, 43, 413–421.

Boisier, J.P., Alvarez-Garreton, C., Cordero, R.R., Damian, A., Gallardo, L., Garreaud, R.D., Lambert, F., Ramallo, C., Rojas, M. and Rondanelli, R. (2018) Anthropogenic drying in Central-Southern Chile evidenced by long term observations and climate model simulations. *Elementa: Science of the Anthropocene*, 6, 74. https://doi.org/10.1525/elementa.328.

Bozkurt, D., Rojas, M., Boisier, J.P. and Valdivieso, J. (2018) Projected hydroclimate changes over Andean basins in Central Chile from downscaled CMIP5 models under the low and high emission scenarios. *Climatic Change*, 150, 131–147.

Cai, W., Purich, A., Cowan, T., van Rensch, P. and Weller, E. (2014) Did climate change–induced rainfall trends contribute to the Australian millennium drought? *Journal of Climate*, 27, 3145–3168.

Capotondi, A., Wittenberg, A.T., Newman, M., Di Lorenzo, E., Yu, J.-Y., Braconnot, P., Cole, J., Dewitte, B., Giese, B. and Guilyardi, E. (2015) Understanding ENSO diversity. *Bulletin of the American Meteorological Society*, 96, 921–938.

Cionni, I., Eyring, V., Lamarque, J., Randel, W., Stevenson, D., Wu, F., Bodeker, G., Shepherd, T., Shindell, D. and Waugh, D. (2011) Ozone database in support of CMIP5 simulations: results and corresponding radiative forcing. *Atmospheric Chemistry and Physics*, 11, 11267–11292.

Clem, K.R. and Fogt, R.L. (2015) South Pacific circulation changes and their connection to the tropics and regional Antarctic warming in austral spring, 1979–2012. *Journal of Geophysical Research Atmosphere*, 120, 2773–2792. https://doi.org/10.1002/2014JD022940.

CR2: Report to the Nation: The Central Chile Mega-Drought. Technical report from the Center for Climate and Resilience Research. 30 pp. Santiago-Chile. Available at: http://www.cr2.cl/megasequia, 2015.

Dai, A. (2011) Drought under global warming: a review. *Wiley Interdisciplinary Reviews: Climate Change*, 2, 45–65.

Dai, A. (2013) Increasing drought under global warming in observations and models. *Nature Climate Change*, 3, 52–58.

Dee, D., Uppala, S.M., Simmons, A.J., Berrisford, P., Poli, P., Kobayashi, S., Andrae, U., Balmaseda, M.A., Balsamo, G., Bauer, P., Bechtold, P., Beljaars, A.C.M., van de Berg, L., Bidlot, J., Bormann, N., Delsol, C., Dragani, R., Fuentes, M., Geer, A.J., Haimberger, L., Healy, S.B., Hersbach, H., Hólm, E.V., Isaksen, L., Kållberg, P., Köhler, M., Matricardi, M., McNally, A. P., Monge-Sanz, B.M., Morcrette, J.-J., Park, B.-K., Peubey, C., de Rosnay, P., Tavolato, C., Thépaut, J.-N. and Vitart, F. (2011) The ERA-interim reanalysis: configuration and performance of the data assimilation system. *Quarterly Journal of the Royal Meteorological Society*, 137, 553–597. https://doi.org/10.1002/qj.828.

Deser, C., Phillips, A., Bourdette, V. and Teng, H. (2012) Uncertainty in climate change projections: the role of internal variability. *Climate Dynamics*, 38, 527–546.

England, M.H., McGregor, S., Spence, P., Meehl, G., Timmermann, A., Cai, W., Gupta, A.S., McPhaden, M., Purich, A. and Santoso, A. (2014) Recent intensification of wind-driven circulation in the Pacific and the ongoing warming hiatus. *Nature Climate Change*, 4, 222–227.

Eyring, V., Arblaster, J., Cionni, I., Sedláček, J., Perlwitz, J., Young, P., Bekki, S., Bergmann, D., Cameron-Smith, P. and Collins, J. (2013) Long-term ozone changes and associated climate impacts in CMIP5 simulations. *Journal of Geophysical Research: Atmospheres*, 118, 5029–5060.

Falvey, M. and Garreaud, R. (2007) Wintertime precipitation episodes in Central Chile: associated meteorological conditions and orographic influences. *Journal of Hydrometeorology*, 8, 171–193.

Fogt, R., Wovrosh, A., Langen, R. and Simmonds, I. (2012) The characteristic variability and connection to the underlying synoptic activity of the Amundsen-Bellingshausen seas low. *Journal of Geophysical Research*, 117, D07111. https://doi.org//10.1029/2011JD017337.

Fuenzalida, H., Aceituno, P., Falvey, M., Garreaud, R., Rojas, M. and Sanchez, R. (2007) *Study on Climate Variability for Chile during the 21st Century. Technical Report*. Santiago, Chile: National Environmental Committee. Available at: http://dgf.uchile.cl/PRECIS. Accessed March 5, 2015.

Fyfe, J., Boer, G. and Flato, G. (1999) The Arctic and Antarctic oscillations and their projected changes under global warming. *Geophysical Research Letters*, 26, 1601–1604.

Garcia-Herrera, R., Hernández, E., Barriopedro, D., Paredes, D., Trigo, R.M., Trigo, I.F. and Mendes, M. (2007) The outstanding 2004/05 drought in the Iberian Peninsula: associated atmospheric circulation. *Journal of Hydrometeorology*, 8, 483–498.

Garreaud, R., Lopez, P., Minvielle, M. and Rojas, M. (2013) Large scale control on the Patagonia climate. *Journal of Climate*, 26, 215–230.

Garreaud, R., Vuille, M., Compagnucci, R. and Marengo, J. (2009) Present-day south american climate. *Palaeogeography, Palaeoclimatology, Palaeoecology*, 281, 180–195.

Garreaud, R. (2007) Precipitation and circulation covariability in the extratopics. *Journal of Climate*, 20, 4789–4797.

Garreaud, R.D., Alvarez-Garreton, C., Barichivich, J., Boisier, J.P., Christie, D., Galleguillos, M., LeQuesne, C., McPhee, J. and Zambrano-Bigiarini, M. (2017) The 2010–2015 megadrought in Central Chile: impacts on regional hydroclimate and vegetation. *Hydrol Earth Syst Sci*, 21, 6307–6327. https://doi.org/10.5194/hess-21-6307-2017.

Gates, W., Boyle, J., Covey, C., Dease, C., Doutriaux, C., Drach, R., Fiorino, M., Gleckler, P., Hnilo, J., Marlais, S., Phillips, T., Potter, G., Santer, B., Sperber, K., Taylor, K. and Williams, D. (1998) An overview of the results of the atmospheric model Intercomparison project (AMIP I). *Bulletin of the American Meteorological Society*, 73, 1962–1970.

Gillett, N., Fyfe, J. and Parker, D. (2013) Attribution of observed sea level pressure trends to greenhouse gas, aerosol, and ozone changes. *Geophysical Research Letters*, 40(10), 2302–2306.

Gillett, N. and Fyfe, J. (2013) Annular mode changes in the CMIP5 simulations. *Geophysical Research Letters*, 40, 1189–1193.

González, M.E., Gómez-González, S., Lara, A., Garreaud, R. and Díaz-Hormazábal, I. (2018) The 2010-2015 Megadrought and its influence on the fire regime in central and south Central Chile. *Ecosphere*, 9, 1–17. https://doi.org/10.1002/ecs2.2300.

González-Reyes, Á., McPhee, J., Christie, D., Le Quesne, C., Szejner, P., Masiokas, M., Villalba, R., Muñoz, A. and Crespo, S. (2017) Spatiotemporal variations in Hydroclimate across the Mediterranean Andes (30°–37° S) since the early twentieth century. *Journal of Hydrometeorology*, 18(7), 1929–1942.

Griffin, D. and Anchukaitis, K.J. (2014) How unusual is the 2012–2014 California drought? *Geophysical Research Letters*, 41, 9017–9023. https://doi.org/10.1002/2014GL062433.

Hoerling, M., Eischeid, J. and Perlwitz, J. (2010) Regional precipitation trends: distinguishing natural variability from anthropogenic forcing. *Journal of Climate*, 23, 2131–2145.

Hoskins, B. and Ambrizzi, T. (1993) Rossby wave propagation on a realistic longitudinally varying flow. *Journal of the Atmospheric Sciences*, 50, 1661–1671.

Hoskins, B. and Karoly, D. (1981) The steady linear response of a spherical atmosphere to thermal and orographic forcing. *Journal of the Atmospheric Sciences*, 38, 1179–1196.

Hurrell, J.W., Hack, J., Shea, D., Caron, J. and Rosinski, J. (2008) A new sea surface temperature and sea ice boundary dataset for the community atmosphere model. *Journal of Climate*, 21, 5145–5153.

Jacques-Coper, M. and Garreaud, R. (2014) Characterization of the 1970s climate shift in South America. *International Journal of Climatology*, 35, 2164–2179. https://doi.org/10.1002/joc.4120.

Jones, J.M., Gille, S., Goosse, H., Abram, N., Canziani, P., Charman, D., Clem, K., Crosta, X., de Lavergne, C. and Eisenman, L. (2016) Assessing recent trends in high-latitude southern hemisphere surface climate. *Nature Climate Change*, 6, 917–926.

Kalnay, E., Kanamitsu, M., Kistler, R., Collins, W., Deaven, D., Gandin, L., Iredell, M., Saha, S., White, G. and Woollen, J. (1996) The NCEP/NCAR 40-year reanalysis project. *Bulletin of the American Meteorological Society*, 77, 437–471.

Kay, J., Deser, C., Phillips, A., Mai, A., Hannay, C., Strand, G., Arblaster, J., Bates, S., Danabasoglu, G. and Edwards, J. (2015) The community earth system model (CESM) large ensemble project: a community resource for studying climate change in the presence of internal climate variability. *Bulletin of the American Meteorological Society*, 96, 1333–1349.

Kelley, C.P., Mohtadi, S., Cane, M., Seager, R. and Kushnir, Y. (2015) Climate change in the Fertile Crescent and implications of the recent Syrian drought. *Proceedings of the National Academy of Sciences*, 112, 3241–3246.

Kucharski, F., Molteni, F., King, M., Farneti, R., Kang, I. and Feudale, L. (2013) On the need of intermediate complexity general circulation models: a "SPEEDY" example. *Bulletin of the American Meteorological Society*, 94, 25–30.

Mao, Y., Nijssen, B. and Lettenmaier, D. (2015) Is climate change implicated in the 2013–2014 California drought? A hydrologic perspective. *Geophysical Research Letters*, 42, 2805–2813.

Marshall, G. (2003) Trends in the southern annular mode from observations and reanalyses. *Journal of Climate*, 16, 4134–4143.

Masiokas, M., Christie, D., Luckman, B. and Nussbaumer, S. (2016) Reconstructing the annual mass balance of the Echaurren Norte glacier (Central Andes, 33.5°S) using local and regional hydroclimatic data. *The Cryosphere*, 10, 927.

Masiokas, M., Villalba, R., Luckman, B. and Mauget, S. (2010) Intra-to multidecadal variations of snowpack and streamflow records in the Andes of Chile and Argentina between 30 and 37 S. *Journal of Hydrometeorology*, 11(3), 822–831.

Masotti, I., Aparicio-Rizzo, P., Yevenes, M., Garreaud, R., Belmar, L. and Farias, L. (2018) The influence of river discharge on nutrient export and phytoplankton biomass off the Central Chile coast (33°-37°S). Seasonal cycle and interannual variability. *Frontiers in Marine Science*, 5, 423. https://doi.org/10.3389/fmars.2018.00423.

Meinshausen, M., Smith, S., Calvin, K., Daniel, J., Kainuma, M., Lamarque, J., Matsumoto, K., Montzka, S., Raper, S. and Riahi, K. (2011) The RCP greenhouse gas concentrations and their extensions from 1765 to 2300. *Climatic Change*, 109(1–2), 213–241.

Miller, A. (1976) The climate of Chile. In: Schwrdtfeger, W. (Ed.) *The Climates of Central and South America*. Amsterdam: Elsevier, pp. 113–145.

Mo, K. and Higgins, R. (1998) The Pacific–south American modes and tropical convection during the southern hemisphere winter. *Monthly Weather Review*, 126, 1581–1596.

Molteni, F. (2003) Atmospheric simulations using a GCM with simplified physical parametrizations. I: model climatology and variability in multi-decadal experiments. *Climate Dynamics*, 20, 175–191.

Montecinos, A., Diaz, A. and Aceituno, P. (2000) Seasonal diagnostic and predictability of rainfall in subtropical South America based on tropical Pacific SST. *Journal of Climate*, 13, 746–758.

Montecinos, A., Kurgansky, M.V., Muñoz, C. and Takahashi, K. (2011) Non-ENSO interannual rainfall variability in Central Chile during austral winter. *Theoretical and Applied Climatology*, 106, 557–568.

Montecinos, A. and Aceituno, P. (2003) Seasonality of the ENSO-related rainfall variability in Central Chile and associated circulation anomalies. *Journal of Climate*, 16, 281–296.

Moss, R.H., Edmonds, J., Hibbard, K., Manning, M., Rose, S., Vuuren, V., Carter, T., Emori, S., Kainuma, M. and Kram, T. (2010) The next generation of scenarios for climate change research and assessment. *Nature*, 463, 747–756.

Muñoz, A., González-Reyes, A., Lara, A., Sauchyn, D., Christie, D., Puchi, R., Urrutia-Jalabert, R., Toledo-Guerrero, I., Aguilera-Betti, I. and Mundo, I. (2016) Streamflow variability in the Chilean temperate-Mediterranean climate transition (35°S–42°S) during the last 400 years inferred from tree-ring records. *Climate Dynamics*, 47, 4051–4066.

Quintana, J. and Aceituno, P. (2012) Changes in the rainfall regime along the extratropical west coast of South America (Chile): 30-43° S. *Atmosfera*, 25, 1–22.

Rasmusson, E. and Carpenter, T. (1982) Variations in tropical sea surface temperature and surface wind fields associated with the southern oscillation/El Niño. *Monthly Weather Review*, 110, 354–384.

Rayner, N., Parker, D., Horton, E., Folland, C., Alexander, L., Rowell, D., Kent, E. and Kaplan, A. (2003) Global analyses of sea surface temperature, sea ice, and night marine air temperature since the late nineteenth century. *Journal of Geophysical Research*, 108 (D14), 4407. https.//doi.org.//10.1029/2002JD002670.

Reynolds, R., Rayner, N., Smith, T., Stokes, D. and Wang, W. (2002) An improved in situ and satellite SST analysis for climate. *Journal of Climate*, 15(13), 1609–1625.

Rivera, J., Penalba, O., Villalba, R. and Araneo, D. (2017) Spatio-temporal patterns of the 2010–2015 extreme hydrological drought across the Central Andes, Argentina. *Water*, 9, 652.

Rondanelli, R., Hatchett, B., Rutllant, J., Bozkurt, D. and Garreaud, R. (2019) Strongest MJO on record triggers extreme Atacama rainfall and warmth in Antarctica. *Geophysical Research Letters*, 46, 3482–3491. https://doi.org/10.1029/2018GL081475.

Rouault, M. and Richard, Y. (2003) Intensity and spatial extension of drought in South Africa at different time scales. *Water SA*, 29, 489–500.

Rutllant, J. and Fuenzalida, H. (1991) Synoptic aspects of the Central Chile rainfall variability associated with the southern oscillation. *International Journal of Climatology*, 11, 63–76.

Saft, M., Western, A., Zhang, L., Peel, M. and Potter, N. (2015) The influence of multiyear drought on the annual rainfall-runoff relationship: an Australian perspective. *Water Resource Research*, 51, 2444–2463. https://doi.org/10.1002/2014WR015348.

Saurral, R., Doblas-Reyes, F. and García-Serrano, J. (2018) Observed modes of sea surface temperature variability in the South Pacific region. *Climate Dynamics*, 50, 1129–1143.

Schubert, S., Stewart, R., Wang, H., Barlow, M., Berbery, E., Cai, W., Hoerling, M., Kanikicharla, K., Koster, R. and Lyon, B. (2016) Global meteorological drought: a synthesis of current understanding with a focus on SST drivers of precipitation deficits. *Journal of Climate*, 29, 3989–4019.

Seager, R., M., Schubert, S., Wang, H., Lyon, B., Kumar, A., Nakamura, J. and Henderson, N. (2015) Causes of the 2011–14 California drought. *Journal of Climate*, 28, 6997–7024.

Seneviratne, S., et al. (2012) In: Field, C.B. , et al. (Eds.) *Managing the Risks of Extreme Events and Disasters to Advance Climate Change Adaptation*. Cambridge, MA: IPCC, Cambridge University Press, pp. 109–230.

Sherwood, S., Meyer, C., Allen, R. and Titchner, H. (2008) Robust tropospheric warming revealed by iteratively homogenized radiosonde data. *Journal of Climate*, 21, 5336–5352.

Smith, T., Reynolds, R., Peterson, T. and Lawrimore, J. (2008) Improvements to NOAA's historical merged land–ocean surface temperature analysis (1880–2006). *Journal of Climate*, 21, 2283–2296.

Solman, S. and Menéndez, C. (2002) ENSO-related variability of the southern hemisphere winter storm track over the eastern Pacific–Atlantic sector. *Journal of the Atmospheric Sciences*, 59, 2128–2141.

Swain, D. (2015) A tale of two California droughts: lessons amidst record warmth and dryness in a region of complex physical and human geography. *Geophysical Research Letters*, 42, 9999–10,003.

Takaya, K. and Nakamura, H. (2001) A formulation of a phase-independent wave-activity flux for stationary and migratory quasigeostrophic eddies on a zonally varying basic flow. *Journal of the Atmospheric Sciences*, 58, 608–627.

Taylor, K., Stouffer, R. and Meehl, G. (2012) An overview of CMIP5 and the experiment design. *Bulletin of the American Meteorological Society*, 93(4), 485–498.

Trigo, R., Gouveia, C. and Barriopedro, D. (2010) The intense 2007–2009 drought in the Fertile Crescent: impacts and associated atmospheric circulation. *Agricultural and Forest Meteorology*, 150, 1245–1257.

Van Dijk, A., Beck, H., Crosbie, R., De Jeu, R., Liu, Y., Podger, G., Timbal, B. and Viney, N. (2013) The millennium drought in Southeast Australia (2001–2009): natural and human causes and implications for water resources, ecosystems, economy, and society. *Water Resource Research*, 49, 1040–1057. https://doi.org/10.1002/wrcr.20123.

Vera, C. and Díaz, L. (2015) Anthropogenic influence on summer precipitation trends over South America in CMIP5 models. *International Journal of Climatology*, 35(10), 3172–3177. https://doi.org/10.1002/joc.4153.

Verbist, K., Amani, A., Mishra, A. and Cisneros, B. (2016) Strengthening drought risk management and policy: UNESCO international hydrological Programme's case studies from Africa and Latin America and the Caribbean. *Water Policy*, 18, 245–261.

Viale, M. and Garreaud, R. (2015) Orographic effects of the subtropical and extratropical Andes on upwind precipitating clouds. *Journal of Geophysical Research: Atmospheres*, 120, 4962–4974.

Viale, M. and Nuñez, M. (2011) Climatology of winter orographic precipitation over the subtropical Central Andes and associated synoptic and regional characteristics. *Journal of Hydrometeorology*, 12, 481–507.

Vicente-Serrano, S., López-Moreno, J., Gimeno, L., Nieto, R., Morán-Tejeda, E., Lorenzo-Lacruz, J., Beguería, S. and Azorin-Molina, C. (2011) A multiscalar global evaluation of the impact of ENSO on droughts. *Journal of Geophysical Research*, 116, D20109. https.//doi.org//10.1029/2011JD016039.

Volkov, D., Lee, S., Landerer, F. and Lumpkin, R. (2017) Decade-long deep-ocean warming detected in the subtropical South Pacific. *Geophysical Research Letters*, 44, 927–936.

Williams, A., Seager, R., Abatzoglou, J., Cook, B., Smerdon, J. and Cook, E. (2015) Contribution of anthropogenic warming to California drought during 2012–2014. *Geophysical Research Letters*, 42, 6819–6828.

You, Y. and Furtado, J. (2017) The role of South Pacific atmospheric variability in the development of different types of ENSO. *Geophysical Research Letters*, 44, 7438–7446.

SUPPORTING INFORMATION

Additional supporting information may be found online in the Supporting Information section at the end of this article.

How to cite this article: Garreaud RD, Boisier JP, Rondanelli R, Montecinos A, Sepúlveda HH, Veloso-Aguila D. The Central Chile Mega Drought (2010–2018): A climate dynamics perspective. *Int J Climatol*. 2019;1–19. https://doi.org/10.1002/joc.6219